Cell Metabolism
Article

Calcium Signaling through CaMKII Regulates Hepatic Glucose Production in Fasting and Obesity

Lale Ozcan,[1] Catherine C.L. Wong,[4] Gang Li,[1] Tao Xu,[4] Utpal Pajvani,[1] Sung Kyu Robin Park,[4] Anetta Wronska,[2] Bi-Xing Chen,[2] Andrew R. Marks,[1,2] Akiyoshi Fukamizu,[5] Johannes Backs,[6] Harold A. Singer,[7] John R. Yates, III,[4] Domenico Accili,[1] and Ira Tabas[1,2,3,*]
[1]Department of Medicine
[2]Department of Physiology and Cellular Biophysics and The Clyde and Helen Wu Center for Molecular Cardiology
[3]Department of Pathology and Cell Biology
Columbia University, New York, NY 10032, USA
[4]Department of Chemical Physiology, Scripps Research Institute, La Jolla, CA 92037, USA
[5]Life Science Center, Tsukuba Advanced Research Alliance, University of Tsukuba, Tsukuba, Ibaraki 305-8577, Japan
[6]Department of Internal Medicine III, Department of Cardiology, University of Heidelberg, 69120 Heidelberg, Germany
[7]Center for Cardiovascular Sciences, Albany Medical College, Albany, NY 12208, USA
*Correspondence: iat1@columbia.edu
DOI 10.1016/j.cmet.2012.03.002

SUMMARY

Hepatic glucose production (HGP) is crucial for glucose homeostasis, but the underlying mechanisms have not been fully elucidated. Here, we show that a calcium-sensing enzyme, CaMKII, is activated in a calcium- and IP3R-dependent manner by cAMP and glucagon in primary hepatocytes and by glucagon and fasting in vivo. Genetic deficiency or inhibition of CaMKII blocks nuclear translocation of FoxO1 by affecting its phosphorylation, impairs fasting- and glucagon/cAMP-induced glycogenolysis and gluconeogenesis, and lowers blood glucose levels, while constitutively active CaMKII has the opposite effects. Importantly, the suppressive effect of CaMKII deficiency on glucose metabolism is abrogated by transduction with constitutively nuclear FoxO1, indicating that the effect of CaMKII deficiency requires nuclear exclusion of FoxO1. This same pathway is also involved in excessive HGP in the setting of obesity. These results reveal a calcium-mediated signaling pathway involved in FoxO1 nuclear localization and hepatic glucose homeostasis.

INTRODUCTION

Liver is the main organ responsible for maintaining euglycemia under conditions of nutrient deprivation. During the early stages of fasting, liver uses glycogen stores to mobilize glucose (Radziuk and Pye, 2001). As fasting progresses, de novo synthesis of glucose from noncarbohydrate precursors, gluconeogenesis, becomes the main contributor to hepatic glucose production (HGP) (Lin and Accili, 2011). These changes occur rapidly in response to direct hormonal signaling. In addition, both insulin and glucagon affect transcription of glucose-6-phosphatase (*G6pc*), which is involved in both gluconeogenesis and glycogenolysis, and phosphoenolpyruvate carboxykinase (*Pck1*), which also regulates HGP (Pilkis and Granner, 1992; Burgess et al., 2007). During fasting, changes in the subcellular localization of "glucogenic" transcription factors, such as FoxO (1, 3, and 4) and Crtc2, activate expression of these genes (Lin and Accili, 2011). In addition, different coactivators, such as peroxisome proliferator-activated receptor-γ coactivator-1α (PGC-1α) and CBP, are thought to interact with components of the cAMP response, including CREB, hepatic nuclear factor 4α (HNF4α), Sirt1, and Clock genes, leading to an increase in transcription of gluconeogenic genes (Hall et al., 1995; Matsumoto et al., 2007; Puigserver et al., 2003; Rhee et al., 2003). In addition to its role in stimulating HGP during fasting, excessive glucagon signaling is thought to play an important role in hyperglycemia in type 2 diabetes (Sørensen et al., 2006; Unger and Cherrington, 2012; Saltiel, 2001).

The intracellular signal transduction pathways through which glucagon stimulates the nuclear translocation of HGP transcription factors in general, and FoxO1 in particular, to stimulate HGP is not well understood. In this context, we became interested in previous reports that linked intracellular calcium (Ca^{2+}_i) to the regulation of gluconeogenesis (Friedmann and Rasmussen, 1970; Kraus-Friedmann and Feng, 1996; Marques-da-Silva et al., 1997). For example, glucagon and cAMP can increase Ca^{2+}_i, and Ca^{2+}_i chelation has been shown to reduce glucagon induced HGP gene expression and glucose production (Bygrave and Benedetti, 1993; Staddon and Hansford, 1989; Mine et al., 1993). Based on these previous studies, which did not offer a molecular mechanism linking Ca^{2+}_i to hepatic glucose metabolism, we conceived a hypothesis implicating a role for the Ca^{2+}_i -sensing enzyme CaMKII.

Calcium calmodulin-dependent kinase II (CaMKII) is a serine-threonine kinase that is an important mediator of Ca^{2+}_i signaling in cells (Couchonnal and Anderson, 2008; Singer, 2011). There are four CaMKII isoforms—α, β, γ, and δ—each encoded by a separate gene. The α and β isoforms are mostly neuronal,

whereas CaMKIIγ and δ are expressed in a wide variety of tissues. After binding calcium/calmodulin complex, autophosphorylation on Thr287 results in calcium/calmodulin independent activity (Couchonnal and Anderson, 2008; Singer, 2011). Most studies on CaMKII have been carried out in neurons and cardiomyocytes, and there is only a limited understanding of CaMKII in other tissues, with none to date related to hepatic glucose metabolism. In the present study, we show that CaMKII activity is increased by cAMP and glucagon and also in response to fasting in vivo. We further demonstrate that CaMKII plays an essential role in the regulation of glycogenolysis and gluconeogenesis. In particular, we provide evidence that CaMKII has a profound effect on FoxO1 nuclear localization in a manner that regulates the expression of two key enzymes, *G6pc* and *Pck1*, in vitro and in vivo. Finally, we present evidence suggesting that this same pathway is involved in excessive HGP in the setting of obesity.

RESULTS

Glucagon and Fasting Activate Hepatic CaMKII in an IP3R- and $Ca^{2+}{}_i$-Dependent Manner

Glucagon has been shown to increase intracellular calcium ($Ca^{2+}{}_i$) in hepatocytes (HCs) (Staddon and Hansford, 1989), which we recently verified (Wang et al., 2012). To determine whether glucagon activates the $Ca^{2+}{}_i$-sensing enzyme, CaMKII, we treated primary murine HCs with glucagon for various periods of time and then assayed CaMKII enzymatic activity and CaMKII phosphorylation at Thr287, which is a measure of its activation state (Couchonnal and Anderson, 2008; Singer, 2011). The results of both assays show that CaMKII activity increases as a function of time of glucagon treatment (Figures 1A and 1B). We used the cytosolic calcium chelator,1,2-bis[2-aminophenoxy]ethane-N,N,N′,N′-tetraacetic acid tetrakis [acetoxymethyl ester] (BAPTA-AM), to determine the role of $Ca^{2+}{}_i$ on CaMKII activation and found that BAPTA-AM markedly decreased glucagon-induced CaMKII phosphorylation (Figure 1C).

Inositol 1,4,5-trisphosphate receptor (IP_3R) channels, located in the endoplasmic reticulum (ER), release Ca^{2+} in response to IP_3 binding and play a major role in intracellular $Ca^{2+}{}_i$ homeostasis. Additional studies have revealed that glucagon-induced PKA phosphorylates and increases IP3R activity, leading to an increase in $Ca^{2+}{}_i$ (Wang et al., 2012). Glucagon has also been shown to induce phospholipase C-mediated IP3 release (Hansen et al., 1998). To investigate the contribution of IP3Rs in glucagon-induced CaMKII activation, we used the IP3R inhibitor xestospongin C and, as a complementary approach, adeno-Cre-treated HCs from *Ip3r1*$^{fl/fl}$ mice. Both xestospongin C treatment and Cre-mediated deletion of IP3R1 led to a significant decrease in glucagon-induced CaMKII phosphorylation, demonstrating the critical role of IP3Rs in this process (Figure 1D).

Glucagon receptor signaling, including that involved in the increase in $Ca^{2+}{}_i$ (Staddon and Hansford, 1989), is mediated by activation of adenylate cyclase to produce cAMP, followed by activation of protein kinase A (PKA), a key enzyme involved in HGP. In this context, we found that treatment of HCs with 8-bromo-cAMP mimicked the effect of glucagon and led to a marked increase in phospho-CaMKII (Figure 1E). Moreover, when HCs were treated with the PKA inhibitor H89 prior to the addition of glucagon, glucagon-mediated increase in phospho-CaMKII was markedly inhibited (Figure 1F). These data support the existence of a pathway in which glucagon-cAMP-PKA signaling promotes phosphorylation/activation of CaMKII through its effects on IP3R-mediated intracellular Ca^{2+} release.

To examine whether CaMKII is regulated by glucagon in vivo, we challenged mice with a bolus of intraperitoneal (i.p.) glucagon. Consistent with the effects observed in cultured HCs, hepatic CaMKII phosphorylation was induced by glucagon treatment (Figure 1G). We found that a glucagon dose as low as 1 μg kg^{-1} was capable of phosphorylating CaMKII in the liver (Figure S1A available online). To gain in vivo evidence that IP3Rs are important in the regulation of glucagon-mediated CaMKII phosphorylation, we treated mice with i.p. xestospongin C for 4 days. The mice were then challenged with glucagon, and liver extracts were assayed for p-CaMKII. As shown in Figure 1H, xestospongin C treatment markedly reduced glucagon-induced CaMKII phosphorylation. Next, we compared hepatic CaMKII phosphorylation during the transition from a fed to fasting state, which is known to elevate plasma glucagon (Lin and Accili, 2011) (Figure S1B). The data show that hepatic CaMKII phosphorylation was significantly increased upon fasting, whereas the total amount of CaMKII appeared to be unaffected by nutrient status (Figure 1I). Moreover, upon refeeding, the level of p-CaMKII in liver diminished (Figure 1J). As with glucagon treatment, fasting-induced phosphorylation of CaMKII was suppressed by xestospongin C treatment of the mice (Figure S1C). These data show that activity of hepatic CaMKII is regulated by nutrient status in a manner that is consistent with a potential role in fasting-induced HGP.

CaMKII Promotes Glucose Production in Primary HCs

CaMKIIγ is the major CaMKII isoform in HCs, and the other isoforms are not induced in HCs lacking the γ isoform (Figure 2A). In view of the regulation of hepatic CaMKII activity by glucagon and fasting in vivo, we assayed glucose production in HCs from wild-type (WT) and *Camk2g*$^{-/-}$ mice. We examined the cells under basal conditions and after stimulation with forskolin, a glucagon mimetic and a potent adenylate cyclase activator (Harano et al., 1985). The data show that both basal and forskolin-induced glucose production was suppressed in CaMKIIγ-deficient HCs (Figure 2B). We next examined glucose production in WT HCs transduced with adenoviruses expressing constitutively active CaMKII (adeno-CA-CaMKII), ''kinase-dead'' dominant-negative CaMKII (adeno-KD-CaMKII) (Pfleiderer et al., 2004), or LacZ control. CA-CaMKII possesses an amino acid substitution, T287D, which mimics autophosphorylation at T287 and results in autonomous activity in the absence of bound calcium/calmodulin, while KD-CaMKII has a disabling mutation in the kinase domain (Pfleiderer et al., 2004). We observed an increase in both basal and forskolin-induced glucose release in cells transduced with adeno-CA-CaMKII (Figure 2C; Figure S1D). HCs transduced with adeno-KD-CaMKII, which resulted in ~40% decrease in CaMKII activity (Figure S1E), showed decreased forskolin-induced glucose production (Figure 2C).

The role of CaMKII on HGP prompted us to investigate transcriptional effects on two genes encoding enzymes that regulate HGP, glucose-6-phosphatase and phosphoenolpyruvate

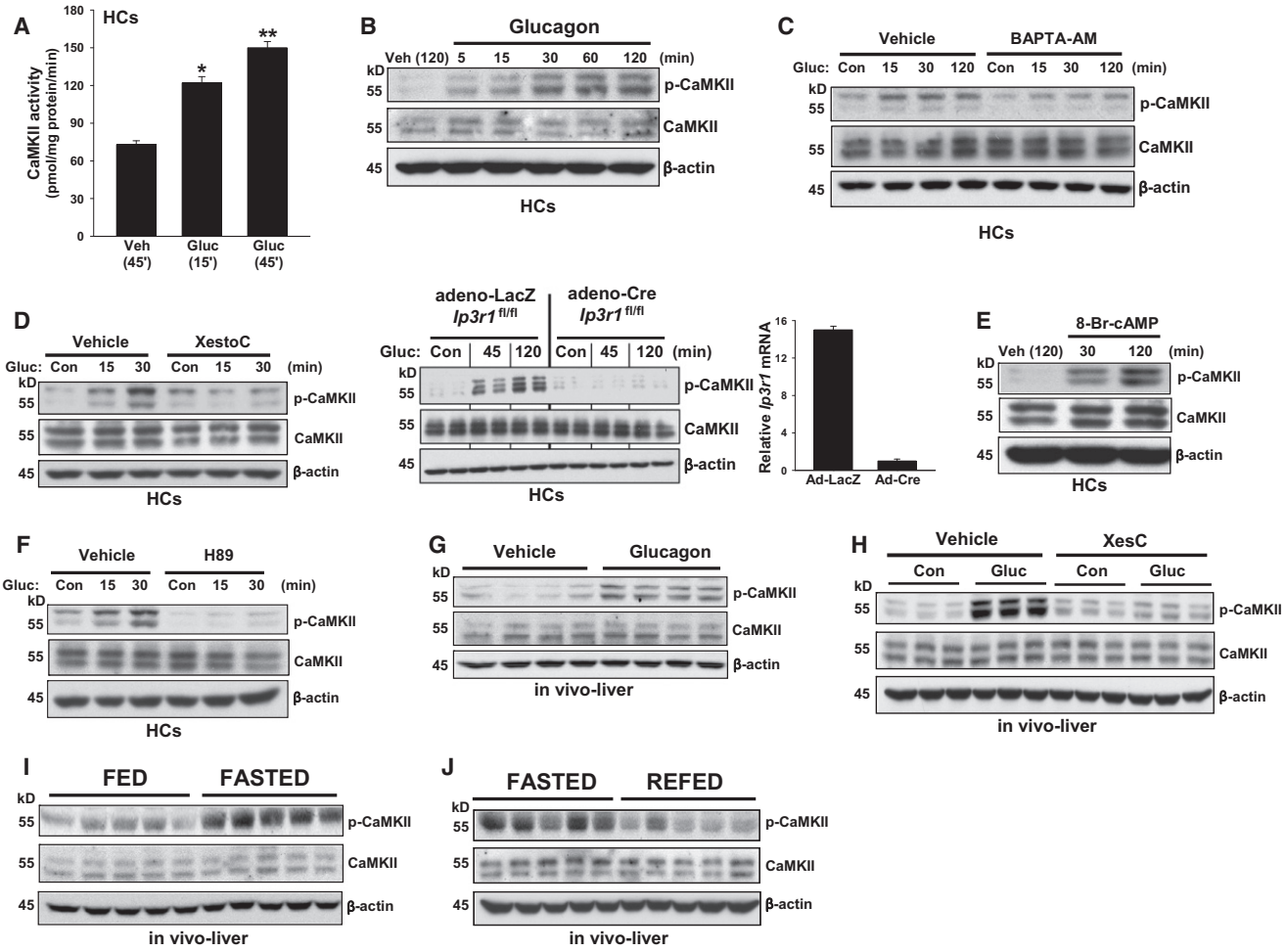

Figure 1. Glucagon and Fasting Activates Hepatic CaMKII

(A) CaMKII enzyme activity was assayed in triplicate wells of primary mouse HCs stimulated with 100 nM glucagon (Gluc) or vehicle control (Veh) for the indicated times (*$p < 0.05$ and **$p < 0.01$ versus Veh; mean ± SEM).

(B–J) Extracts of HCs or liver were probed for phospho-CaMKII, total CaMKII, and β-actin by immunoblot assay. HCs were incubated with 100 nM glucagon for the indicated times (B). Glucagon was added to HCs that were pretreated for 1 hr with vehicle control (Veh) or 5 μM BAPTA-AM (C). Glucagon was added to HCs that were pretreated with 0.5 μM xestospongin (XesC) or to HCs from *Ip3r1*$^{fl/fl}$ mice transduced with adeno-LacZ control or adeno-Cre (bar graph = *Ip3r1* mRNA levels) (D). Glucagon was added to HCs that were pretreated for 1 hr with vehicle control (Veh) or 10 μM H89 (E). HCs were incubated with 100 μM 8-bromo-cAMP for the indicated times (F). In vivo experiments are shown in (G)–(J). In (G), mice were treated for 30 min with 200 μg kg^{-1} body weight of glucagon i.p., and in (H), mice were pretreated with 10 pmol g^{-1} xestospongin C or vehicle control i.p. 4 days prior to glucagon treatment. In (I) and (J), mice were fed ad libitum or fasted for 12 hr, or fasted for 12 hr and then refed for 4 hr. See also Figure S1 and Table S1.

carboxykinase. To this end, we assayed *G6pc* and *Pck1* mRNA levels in the models described above (Figures 2D and 2E). In all cases, knockout or KD-CaMKII-mediated inhibition of CaMKII lowered forskolin- or glucagon-induced gene expression, whereas CA-CaMKII increased gene expression. In the absence of forskolin or glucagon, expression levels of *G6pc* and *Pck1* mRNA in WT HCs were much lower than those in hormone-treated WT HCs, but even under these conditions CaMKIIγ deficiency led to a lowering of gene expression (Figure S1F). Moreover, adeno-KD-CaMKII did not decrease the low but detectable level of forskolin-induced *G6pc* mRNA in HCs lacking CaMKIIγ (Figure S1G), consistent with the premise that the suppressive effect of KD-CaMKII on *G6pc* in Figure 2E is due to CaMKII inhibition.

In summary, the CaMKII deficiency and inhibition data show the importance of endogenous CaMKII in glucose production and *Pck1*/*G6pc* gene expression, while the data with CA-CaMKII show that when the enzyme is expressed at a high level, it can force these processes in the absence of hormones or increase them in the presence of hormones.

Hepatic Glucose Production In Vivo Is Impaired by CaMKIIγ Deficiency and Stimulated by Constitutively Active CaMKII

To assess the functional role of CaMKII in hepatic glucose metabolism in vivo, we first examined fasting blood glucose levels in WT and *Camk2g*$^{-/-}$ mice. Consistent with our in vitro data, we observed a modest but statistically significant decrease

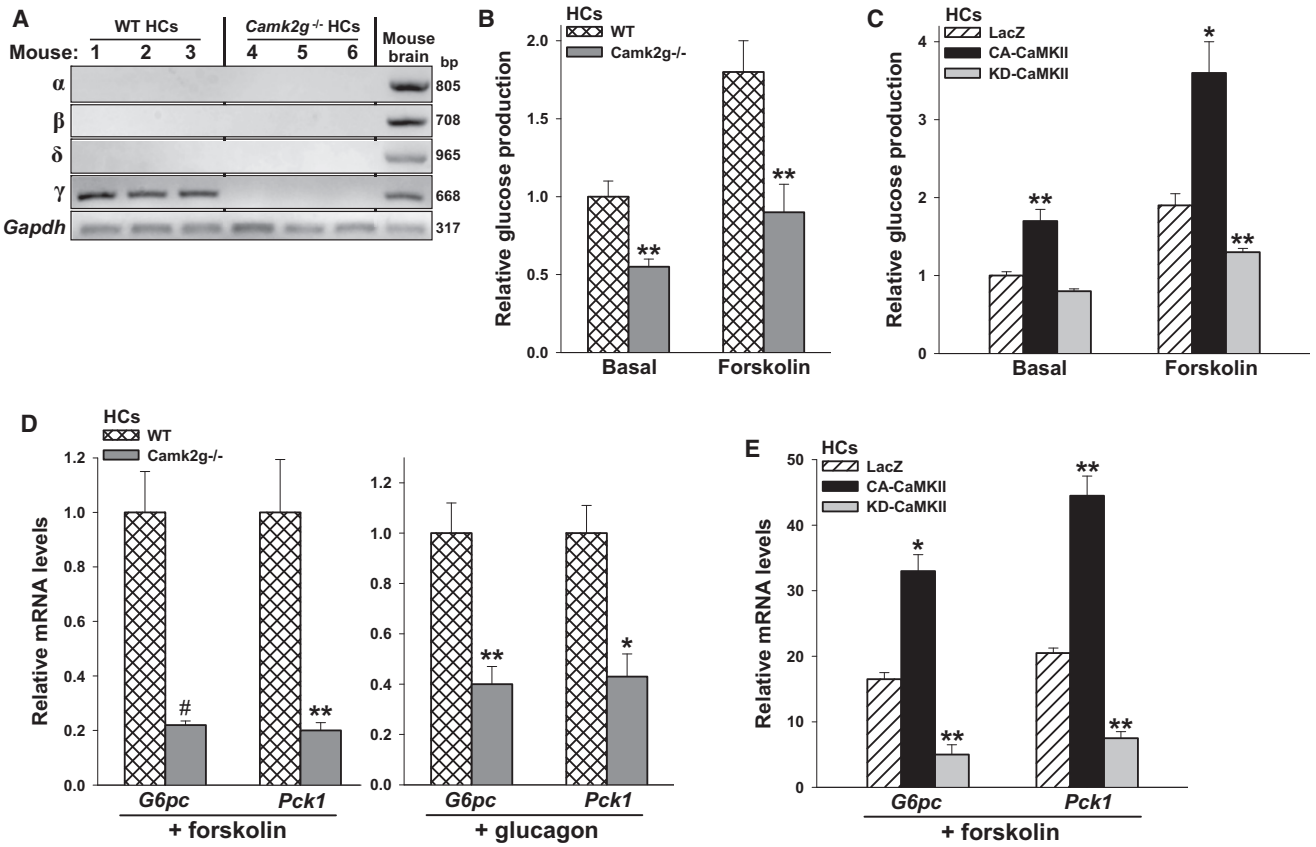

Figure 2. CaMKII Regulates Glucose Production and Hepatic *G6Pc* and *Pck1* Expression in Primary HCs

(A) RNA from HCs from three WT and three *Camk2g*$^{-/-}$ mice and mouse brain from a WT mouse were probed for the indicated *Camk2* isoform mRNAs by RT-PCR.

(B) HCs from WT and *Camk2g*$^{-/-}$ mice were serum-depleted overnight and then incubated with forskolin (10 μm) for 14 hr in serum- and glucose-free media, and then glucose in the medium was assayed (**p < 0.01 versus WT in each group; mean ± SEM).

(C) HCs from WT mice were transduced with adenoviral vectors expressing LacZ, CA-CaMKII, or KD-CaMKII at an MOI of 20 and then assayed for glucose production as in (B) (*p < 0.05 and **p < 0.01 versus LacZ in each group; mean ± SEM).

(D and E) HCs similar to those in (B) and (C) were serum-depleted overnight and then incubated for 5 hr with 10 μM forskolin or 100 nM glucagon in serum-free media, as indicated. RNA was assayed for *G6pc* and *Pck1* mRNA by RT-qPCR (*p < 0.05 and **p < 0.01 versus LacZ or WT in each group; mean ± SEM). See also Figure S2 and Table S1.

in blood glucose levels in fasted *Camk2g*$^{-/-}$ versus WT mice (Figure 3A). The difference in fasting glucose concentration was not associated with an increase in circulating insulin or a decrease in glucagon concentrations in knockout versus WT mice (Figure S2A, left). The mutant mice also showed lower plasma glucose in response to a pyruvate challenge test (Figure 3B). Consistent with the primary HC data, there was a decrease in *G6pc* and *Pck1* mRNA levels in the livers of fasting *Camk2g*$^{-/-}$ mice (Figure 3C). Similar data were obtained in mice treated with glucagon (Figure 3D).

Consistent with these data, treatment of C57BL/6 mice with adeno-KD-CaMKII, which inhibited liver CaMKII activity by ~45% (Figure S2B), decreased fasting blood glucose (Figure 3E). As above, plasma glucagon and insulin were not different between the control and experimental groups (Figure S2A, right). In line with blood glucose data, hepatic expression of *G6pc* and *Pck1* mRNA was lower in mice injected with KD-CaMKII (Figure 3F). Because CaMKII inhibition lowers the level of the mRNA for the key glycogenolytic enzyme glucose-6-phosphatase, we examined the effect of acute and chronic CaMKII inhibition on liver glycogen content and, as another indicator of glycogen, the percent of periodic acid-Schiff (PAS)-positive cells. The data show that adeno-KD-CaMKII or CaMKII gene targeting increases hepatic glycogen in fasting mice (Figure 3G).

We next examined the effect of constitutively active hepatic CaMKII in mice by treating mice with adeno-CA-CAMKII. The CA-CaMKII group had elevated blood glucose levels after pyruvate challenge, increased liver *G6pc* and *Pck1* mRNA levels, and increased liver glycogen content (Figures S2C–S2E). CA-CaMKII administration did not alter plasma glucagon or insulin (data not shown). These combined in vivo data show that CaMKII affects plasma glucose levels, pyruvate conversion into glucose, and the expression of hepatic glucose metabolism genes.

CaMKII Promotes Nuclear Localization of FoxO1

A major transcription factor involved in HGP is FoxO1, which is regulated primarily by changes in its localization between the cytoplasm and nucleus (Accili and Arden, 2004). We therefore

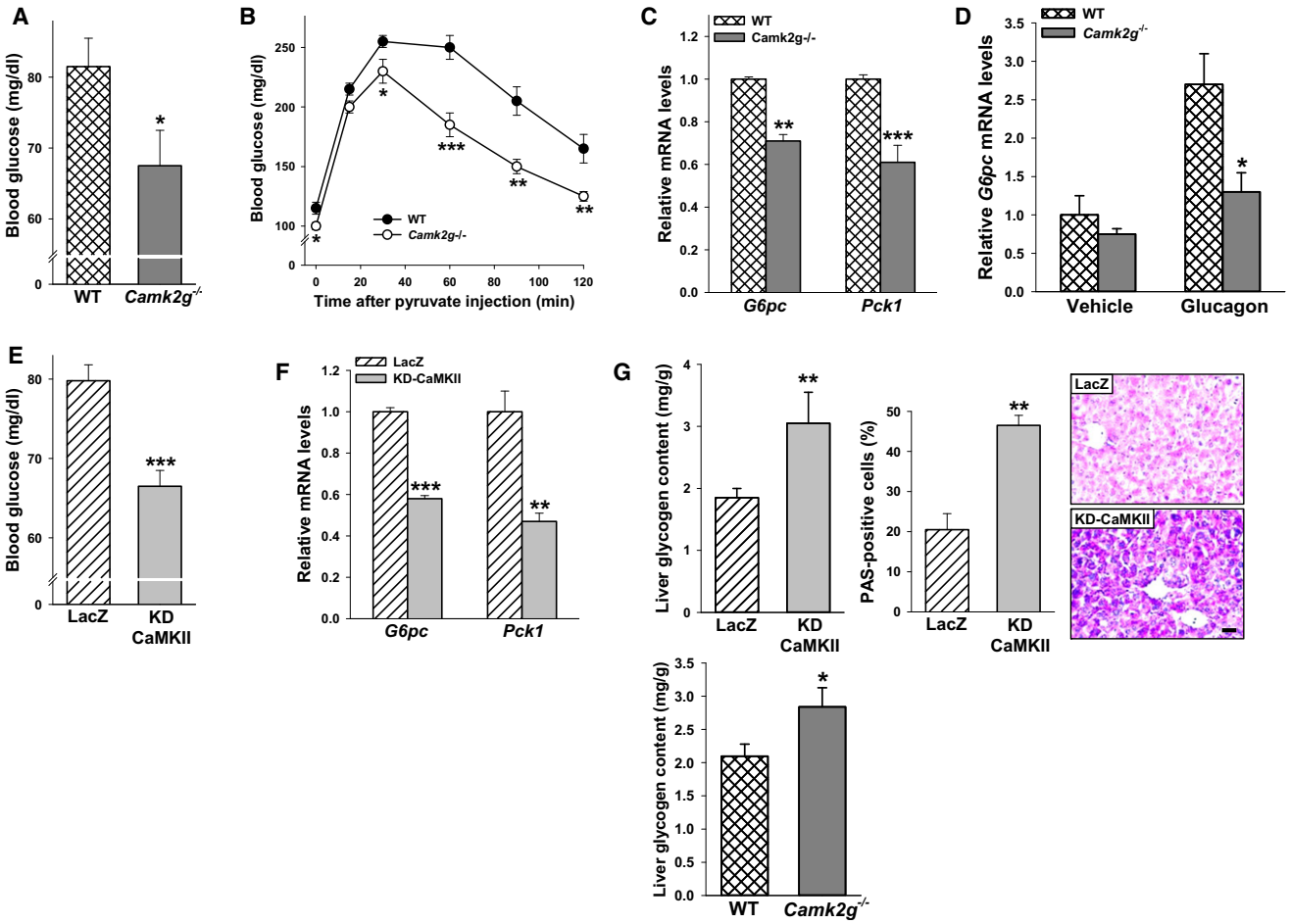

Figure 3. CaMKIIγ Deficiency or Acute Inhibition In Vivo Decreases Blood Glucose and Hepatic *G6pc* and *Pck1*

(A) Blood glucose of 12-hr-fasted 8-week-old WT and *Camk2g*$^{-/-}$ mice (*$p < 0.05$).

(B) As in (A), but the mice were fasted for 18 hr and then challenged with 2 mg kg^{-1} pyruvate (B) (*$p < 0.05$; **$p < 0.01$; ***$p < 0.005$; mean ± SEM).

(C) Liver *G6pc* and *Pck1* mRNA in 12-hr-fasted WT and *Camk2g*$^{-/-}$ mice (**$p < 0.01$; ***$p < 0.001$; mean ± SEM).

(D) WT and *Camk2g*$^{-/-}$ mice were injected i.p. with glucagon (200 μg kg^{-1}) and sacrificed 30 min later. Liver *G6pc* mRNA was assayed (*$p < 0.05$; mean ± SEM).

(E–G) Nine-week-old WT mice were administered 1.5 × 10^{9} pfu of adeno-LacZ or KD-CaMKII, and 5 days later the following parameters were assayed in 12-hr-fasted mice: blood glucose (E, ***$p < 0.001$; mean ± SEM), liver *G6pc* and *Pck1* mRNA (F, **$p < 0.01$; ***$p < 0.001$; mean ± SEM), and liver glycogen content and PAS-positive cells (G, **$p < 0.01$; mean ± SEM). (G) also shows liver glycogen content in fasted WT and *Camk2g*$^{-/-}$ mice (*$p < 0.05$; mean ± SEM). For all panels, n = 5/group except in (D), where n = 4/group.

assayed the distribution of GFP-tagged FoxO1 that was transduced into HCs isolated from WT versus *Camk2g*$^{-/-}$ mice. Under serum-starved conditions, the majority of GFP-FoxO1 was in the nucleus in WT HCs, whereas *Camk2g*$^{-/-}$ HCs displayed primarily cytosolic localization of GFP-FoxO1 (Figure 4A). Moreover, when HCs were transduced with adeno-CA-CaMKII, FoxO1 became predominantly nuclear, while transduction with adeno-KD-CaMKII caused mostly cytoplasmic FoxO1 (Figure 4B). We noted that nuclear FoxO1 was substantial in cultured HCs under the "basal" cell culture conditions used here, and so the fold increase with CA-CaMKII was limited. We therefore lowered basal nuclear FoxO1 using short incubations with insulin, which then revealed a marked increase in nuclear FoxO1 with CA-CaMKII (Figure 4C). Although this experiment was done using a high level of total CaMKII protein expression (see Figure S1D), a similar experiment using a lower multiplicity of infection (MOI) of CA-CaMKII showed an increase in nuclear FoxO1 at a level of total CaMKII protein that was similar to endogenous CaMKII (Figure S3A). To show relevance in vivo, we tested the effect of CaMKIIγ deficiency or inhibition in fasting mice. Nuclear FoxO1 in liver was prominent under fasting conditions (Figure 4D, top blot), and it was markedly diminished in *Camk2g*$^{-/-}$ mice or mice transduced with adeno-KD-CaMKII (Figure 4D, middle two blots). Feeding diminished nuclear FoxO1, and nuclear FoxO1 was increased under these conditions by both CA-CaMKII and glucagon (Figure 4D, bottom blots).

cAMP-mediated induction of *G6pc* mRNA in primary hepatocytes is suppressed ≥50% by *Foxo1* shRNA, suggesting an important role for FoxO1 in the endogenous setting (Matsumoto et al., 2007). Consistent with these data, we found that induction of luciferase downstream of the human *G6PC* promoter was blunted when three consensus FoxO-binding sites were mutated

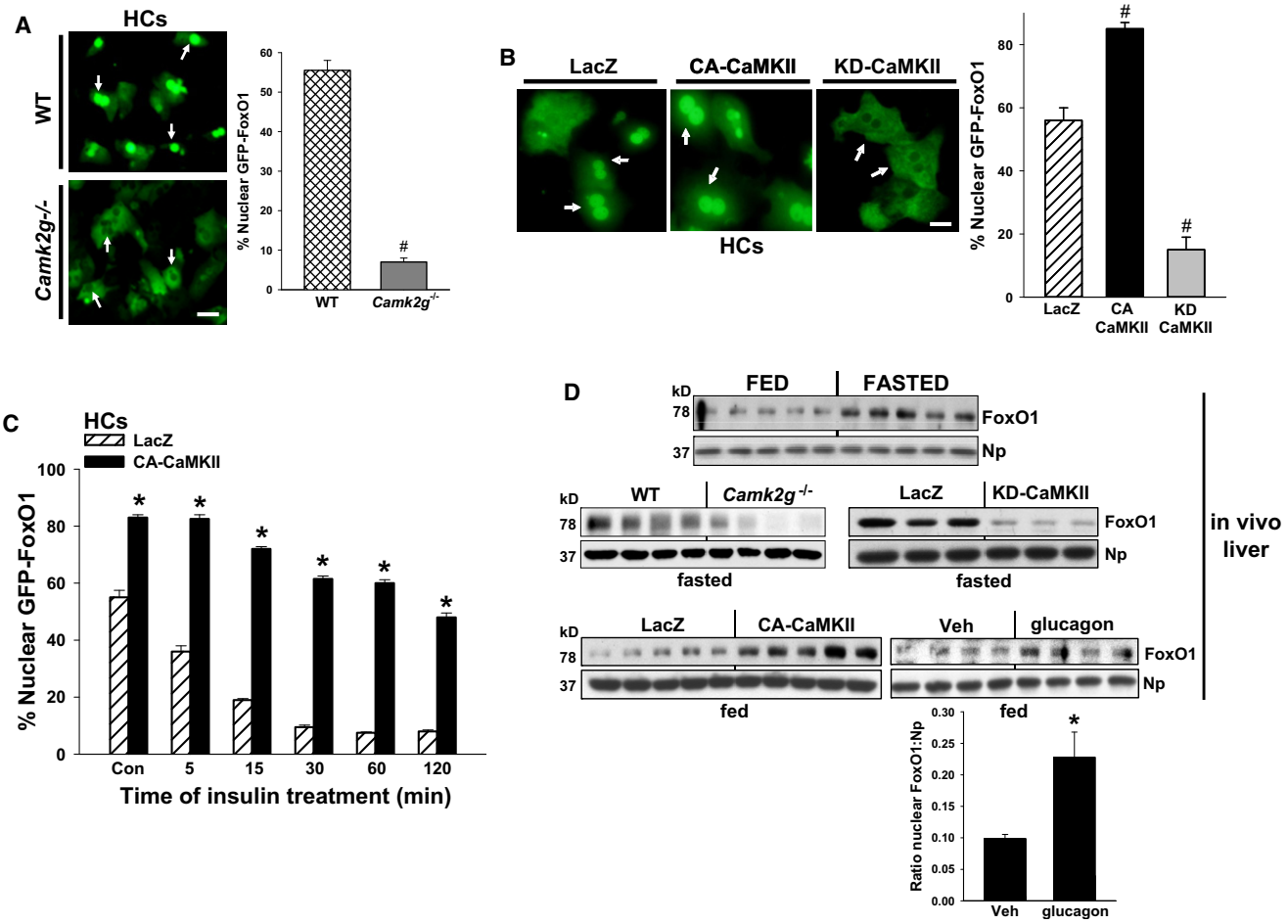

Figure 4. CaMKII Regulates Hepatic FoxO1 Subcellular Localization

(A) HCs from WT and *Camk2g*$^{-/-}$ mice were transduced with an adenovirus expressing murine GFP-FoxO1 at an MOI of 2. Cells were serum-depleted overnight and then incubated for 5 hr in serum-free media. FoxO1 subcellular localization was assessed by indirect immunofluorescence. Bar, 10 μm. Data are quantified in the right panel. ($^{\#}p < 0.0005$; mean ± SEM).

(B) HCs were transduced with adenoviral vectors expressing LacZ, CA-CaMKII, or KD-CaMKII at an MOI of 20 and then transduced 4 hr later with adeno-GFP-FoxO1, followed by fluorescence microscopy and quantification as in (A) ($^{\#}p < 0.005$ versus LacZ; mean ± SEM). Bar, 5 μm.

(C) HCs were transduced with adeno-LacZ or CA-CaMKII and then adeno-GFP-FoxO1 as in (B). After incubation in serum-depleted medium overnight and then serum-free medium for 5 hr, the cells were treated with 100 nM insulin for the indicated times. FoxO1 subcellular localization was quantified as in (B) ($^{*}p < 0.005$ versus LacZ in each group; mean ± SEM).

(D) Nuclear FoxO1 and nucleophosmin were probed by immunoblot in livers from fasted WT mice, *Camk2g*$^{-/-}$ mice, or WT mice treated with adeno-LacZ or KD-CaMKII; from fed WT mice treated with adeno-LacZ or CA-CaMKII; or from fed WT mice treated for 30 min with 200 μg kg^{-1} body weight of glucagon i.p. For the glucagon experiment, the average FoxO:Np densitometric ratio values are in the graph ($^{*}p = 0.029$; blemishes in lanes 6 and 8 were excluded from the densitometry analysis). See also Figure S3 and Table S2.

(Ayala et al., 1999; von Groote-Bidlingmaier et al., 2003) (Figure S3B). However, this hepatoma cell line—reporter construct experiment does not distinguish between cAMP and dexamethasone effects and may not accurately reflect the endogenous situation. For example, reporter induction here was much less robust than actual *G6pc* mRNA induction in primary hepatocytes (Matsumoto et al., 2007), and the identified promoter element may not be the only site required for regulation. Therefore, rather than pursue this model further as a way to assess the functional importance of FoxO1 in CaMKII-mediated *G6pc* expression, we instead focused on induction of endogenous *G6pc* in primary hepatocytes and, most importantly, in vivo. To begin, we compared the ability of CA-CaMKII to induce *G6pc* in HCs from WT versus L-Foxo1 knockout (KO) mice, which lack FoxO1 in liver (Matsumoto et al., 2007). Consistent with previous studies (Puigserver et al., 2003; Matsumoto et al., 2007), forskolin-induced expression of *G6pc* was suppressed in the absence of FoxO1 (Figure 5A, right graph). Most importantly, the increase in *G6pc* mRNA expression by CA-CaMKII was markedly blunted by FoxO1 deficiency. In the absence of forskolin, gene expression was much lower as expected (Figure 5A, left graph; note y axis scale), but even here CA-CaMKII-induced gene expression was almost completely dependent on FoxO1. Finally, we documented that the nuclear localization of two other transcription factors involved in HGP, CREB, and Crtc2, were not decreased by CaMKII inhibition or deficiency (Figures S3C and S3D). These

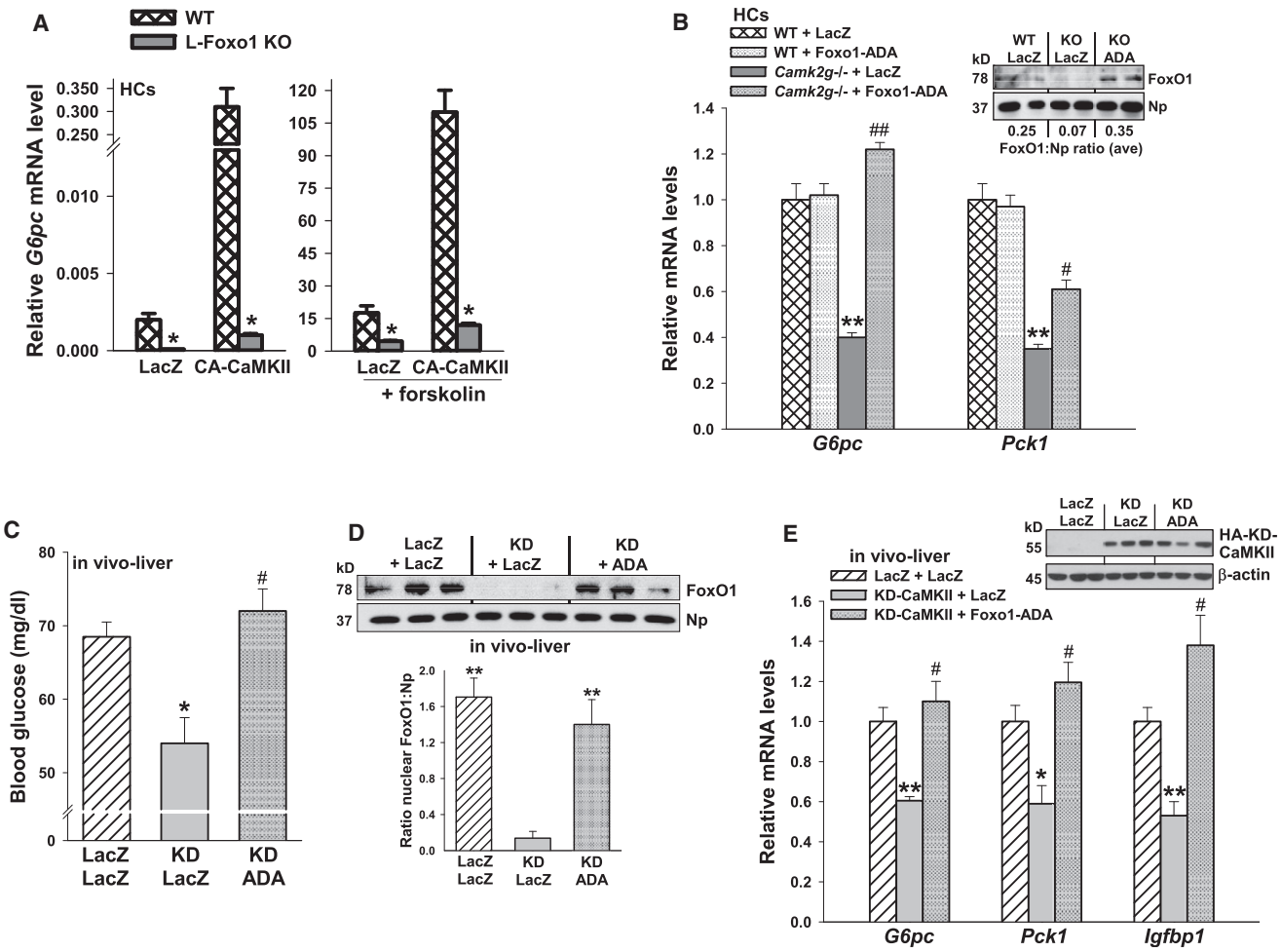

Figure 5. Impairment of Glucose Metabolism by CaMKII Inhibition Is Rescued by Transduction with Constitutively Nuclear FoxO1-ADA

(A) HCs from WT or L-FoxO1 knockout mice were transduced with adeno-LacZ or CA-CaMKII. The cells were serum-depleted overnight and then incubated for 5 hr in the absence or presence of forskolin (10 μm) in serum-free media. RNA was assayed for *G6pc* mRNA (*p < 0.001; mean ± SEM).

(B) HCs from WT and *Camk2g*$^{-/-}$ mice were administered adeno-LacZ or FoxO1-ADA at an MOI of 0.2. Cells were serum-depleted overnight and then incubated for 5 hr with 10 μM forskolin in serum-free media. RNA was assayed for *G6pc* and *Pck1* mRNA (**p < 0.01 versus WT groups; $^{\#}$p < 0.05 and $^{\#\#}$p < 0.01 versus *Camk2g*$^{-/-}$/LacZ group; mean ± SEM). Inset, the nuclei from a parallel set of cells were probed for FoxO1 and nucleophosmin by immunoblot; the average densitometric ratio appears below each pair of lanes.

(C–E) Eight-week-old WT mice were administered adeno-LacZ or KD-CaMKII, and then, one day later, half of the adeno-KD-CaMKII mice received adeno-FoxO1-ADA, while the other half received adeno-LacZ control. Blood glucose levels were assayed at day 5 after a 12-hr fast (*p < 0.05 versus LacZ/LacZ; $^{\#}$p < 0.05 versus KD/LacZ; n = 5/group; mean ± SEM), and liver was assayed for nuclear FoxO1 protein (**p ≤ 0.01 versus KD/LacZ; mean ± SEM); *G6pc*, *Pck1* and *Igfbp1* mRNA (*p < 0.05 and **p < 0.01 versus LacZ/LacZ; $^{\#}$p < 0.05 versus KD/LacZ; n = 3/group; mean ± SEM). The inset in (E) shows the level of hemagglutinin (HA)-tagged KD-CaMKII protein (anti-HA immunoblot). See also Figure S4.

combined data are consistent with a model in which CaMKII promotes FoxO1 nuclear localization, which then leads to induction of *G6pc*.

To further validate the importance of FoxO1 in the impairment of HGP by CaMKII deficiency or inhibition, we transduced HCs from *Camk2g*$^{-/-}$ mice with adenovirus containing a phosphorylation-defective, constitutively nuclear FoxO1 mutant (FoxO1-ADA) (Nakae et al., 2001). We observed that the suppressive effect of CaMKIIγ deficiency on forskolin-induced *G6pc* and *Pck1* mRNA expression was abrogated by transduction with adeno-FoxO1-ADA (Figure 5B). Note that the level of FoxO1-ADA used here was low enough so as not to increase *G6pc* or *Pck1* in forskolin-treated WT HCs, and the level of nuclear FoxO1 in the *Camk2g*$^{-/-}$ + ADA group was similar to the endogenous level in the WT + LacZ group (inset, Figure 5B). The *Pck1* results in Figure 5B, as well as those in Figures 2 and 3, are interesting in view of the finding that germline knockdown of FoxO1 does not affect *Pck1* induction (Nakae et al., 2002; Barthel et al., 2001). However, more acute silencing of FoxO1 does suppress *Pck1* (Matsumoto et al., 2007), and so manipulations of CaMKII may be more parallel to that setting. Consistent with the effect of FoxO1-ADA on HGP gene expression, treatment of mice with adeno-FoxO1-ADA adenovirus rescued the impairment of glucose homeostasis in adeno-KD-CaMKII-treated mice (Figures 5C–5E). Note that this result cannot be explained by defective transduction with adeno-KD in the ADA group (inset,

Figure 5E). Taken together, these results are consistent with a model in which CaMKII contributes to HGP through promoting nuclear localization of FoxO1.

The Role of Non-AKT-Phospho-FoxO1 Sites and p38 MAP Kinase in CaMKIIγ-Mediated FoxO1 Nuclear Localization

Insulin/Akt promotes FoxO1 nuclear exclusion through phosphorylation of T24, S253, and S316 (murine residues) (Brunet et al., 1999). Although CaMKII is a kinase, it could activate a phosphatase and thereby promote nuclear localization of FoxO1 by indirectly decreasing the phosphorylation at these sites. However, we found that phosphorylation at these three sites was not altered in liver from *Camk2g*$^{-/-}$ mice (Figure S4A). FoxO1 acetylation, which can also affect FoxO1 localization and activity in HCs (Accili and Arden, 2004), was also not affected by CaMKII deficiency (Figure S4B).

FoxO1 can also be phosphorylated at other Ser/Thr residues by other kinases, such as p38 MAP kinase (Asada et al., 2007), and these phosphorylation events might promote FoxO1 nuclear localization, not exclusion. To assess the possible role of CaMKII in the phosphorylation of non-Akt sites, we used the model displayed in Figure 4A, i.e., serum-starved WT and *Camk2g*$^{-/-}$ (KO) HCs transduced with GFP-FoxO1, which also carries a FLAG tag. FoxO1 was immunopurified using anti-FLAG, followed by reduction, alkylation, and proteolytic digestion using a triple protease protocol developed by MacCoss et al. (2002). Phosphorylated peptides were enriched by TiO_2 chromatography and then analyzed by LC-MS/MS (Cantin et al., 2007) using MS-based shotgun proteomic methods and label-free quantitation by spectral counting (Cantin et al., 2007). The FoxO1 protein was identified with ~70% sequence coverage, and a total of 57 phosphopeptides for WT and 63 phosphopeptides for KO samples were identified (Tables S1 and S2). The peptide false discovery rate (FDR) was less than 1%. Stringent selection criteria were used so that all identified phosphopeptides would have high confidence.

These criteria, with further validation using the phosphopeptide analysis tools Debunker and Ascore (Lu et al., 2007; Beausoleil et al., 2006), enabled the identification of 11 phosphorylation sites: S284, S295, S326, S467, S475, T24, S246, S253, S413, S415, and T553 (see Figure S4C for murine FoxO1 sequence). Figure 6A shows the spectral counts, the Debunker score, and Ascore of each of these 11 FoxO1 phosphopeptides from the KO and WT samples. Most phosphorylation sites are well above the high confidence cutoff values of 0.5 and 12 for Debunker and Ascore, respectively. Five sites with slightly lower values of Debunker or A scores were subjected to manual verification, and their annotated tandem mass spectra are shown in Figures S5D and S5E for KO peptides 4 and 5 and the aforementioned website for WT peptides 7, 10, and 11. The characteristic b- and/or y-ions for the phospho-sites are all identified. The lower scores are most likely due to the low-abundance fragment ions or lack of neutral losses of phosphoric acid because of the nature of the amino acid sequence for these peptides.

The ratio of spectral KO:WT counts, which was calculated only for peptides with a combined spectral count in KO and WT samples above 10, was used to obtain a measure of the relative expression of identified phosphorylated peptides. By this analysis, only phosphorylation of S295, S467, S475 (peptides 2, 4, and 5) were significantly lower in the KO based on a cutoff value of $\leq$0.5, with the ratio of spectral counts in KO versus WT of 0.45, 0.38, and 0.5, respectively. Although the peptide containing p-S246 had a combined spectral count of 7, and thus did not reach the prespecified criterion of >10, it showed a lower trend in the KO versus WT (2 versus 5, 0.4). In contrast, S326 (peptide 3) had a ratio of 1.65, indicating upregulation in KO versus WT.

As an initial test of function for the some of the sites lower in the KO, we used an available plasmid encoding FoxO1 with S-A mutations at seven Ser residues (7A-FoxO1), including Ser295 and 475, as well as Ser246 (Asada et al., 2007). When transfected to a similar levels in *Foxo1*$^{-/-}$ HCs, 7A-FoxO1 showed strikingly less nuclear localization than WT FoxO1 in response to glucagon, while cytoplasmic FoxO1 was higher in the cells transfected with the mutant FoxO1 (Figure 6B). We also tested a construct that had the same seven S-A mutations as in 7A plus 2 additional S-A mutations in S326 and S467 (mutant 9A) (Asada et al., 2007). This mutant showed similarly defective nuclear localization (Figure S4F). Moreover, whereas adeno-CA-CaMKII transduction increased nuclear WT-FoxO1, consistent with the data in Figure 4D, CA-CaMKII did not increase nuclear 7A-FoxO1 (Figure 6C). These combined data are consistent with a model in which CaMKII directly or indirectly alters the phosphorylation of certain Ser residues in FoxO1 in a manner that promotes its nuclear localization.

Asada et al. (2007) found evidence of FoxO1 phosphorylation at several sites, including Ser284, 295, 467, and 475, in HEK293T cells transfected with the upstream p38 kinase MKK6. Because p38 has been implicated in the stimulation of HGP (Cao et al., 2005), and CaMKII can activate p38 when studied in neurons (Blanquet, 2000), we considered the possibility of a CaMKII → p38 → FoxO1 phosphorylation/nuclear localization pathway involved in HGP. We first confirmed that p38 was phosphorylated, which is a measure of its activation, in the livers of fasting mice (Figure S5A) and that inhibition of p38 by the high-affinity competitive inhibitor SB202190 blocked the expression of *G6pc* and *Pck1* in glucagon-stimulated HCs (Figure S5B, left). The inhibitor data were confirmed using adeno-Cre-transduced HCs isolated from the livers of from *P38a*$^{fl/fl}$ mice (Figure S5B, right). To test a potential link between CaMKII and p38, we compared serum-starved HCs from WT and *Camk2g*$^{-/-}$ mice and found a striking decrease in phospho-p38 in the CaMKIIγ-deficient HCs (Figure S5C). We then determined whether p38 was involved in hepatic FoxO1 nuclear localization in vivo by comparing fasting mice treated with SB202190 versus vehicle control. Among the 7 mice in each group, there was a certain degree of variability in both the basal level of p-MK2, a p38 kinase target that reflects p38 activity, and in the level of inhibition of MK2 phosphorylation by SB202190. We therefore plotted nuclear FoxO1 for all 14 mice as a function of p-MK2. The data show a clear decrease in nuclear FoxO1 in mice as a function of p38 inhibition, i.e., as indicated by lower p-MK2 (Figure S5D). Moreover, the p38 inhibitor decreased nuclear GFP-FoxO1 in HCs treated with glucagon (Figure S5E). These combined data are consistent with a model in which CaMKII promotes FoxO1 nuclear localization through p38 activation. Whether p38 functions in CaMKII-induced FoxO1 nuclear localization by directly

A

Peptide*	Site	Spectral Count # (KO)	Debunker Score (KO)	A Score (KO)	Spectral Count # (WT)	Debunker Score (WT)	A Score (WT)	Spectral Count # Ratio (KO/WT)
1: K.KASLQSGQEGPGDS$^{\Delta}$PGSQFSK.W	**S284**	**4**	**0.99**	**30.66**	**6**	**0.99**	**57.5**	**-**
2: K.WPAS$^{\Delta}$PGSHSNDDFDNWSTFRPR.T	**S295**	**17**	**0.99**	**29.82**	**37**	**0.99**	**40.35**	**0.45**
3: R.TSSNASTISGRLS$^{\Delta}$PIMTEQDDLGDGDVHSLVYPPSAAK.M	**S326**	**33**	**0.90**	**30.65**	**20**	**0.60**	**24.89**	**1.65**
4: K.ELLTSDS$^{\Delta}$PPHNDIMSPVDPGVAQPNSR.V	**S467**	**5**	***0.34***	**16.22**	**13**	**0.59**	**12.09**	**0.38**
5: K.ELLTSDSPPHNDIMS$^{\Delta}$PVDPGVAQPNSR.V	**S475**	**5**	***0.34***	**32.44**	**10**	**0.72**	**44.72**	**0.5**
6: R.SCT$^{\Delta}$WPLPR.P	**T24**	**0**	**0**	**0**	**1**	**0.80**	**42.68**	**-**
7: K.SSWWMLNPEGGKSGKS$^{\Delta}$PR.R	**S246**	**2**	**0.99**	**16.23**	**5**	**0.99**	***10.49***	**-**
8: R.AAS$^{\Delta}$MDNNSKFAKSR.G	**S253**	**3**	**0.99**	**45.45**	**1**	**0.99**	**31.85**	**-**
9: C.YSFAPPNTSLNS$^{\Delta}$PSPNYSK.Y	**S413**	**0**	**0**	**0**	**1**	**0.31**	**14.42**	**-**
10: C.YSFAPPNTSLNSPS$^{\Delta}$PNYSK.Y	**S415**	**0**	**0**	**0**	**1**	**0.92**	***11.56***	**-**
11: R.TLPHVVNTMPHTSAMNRLT$^{\Delta}$PVK.T	**T553**	**2**	**0.99**	**37.41**	**1**	***0.36***	**12.03**	**-**

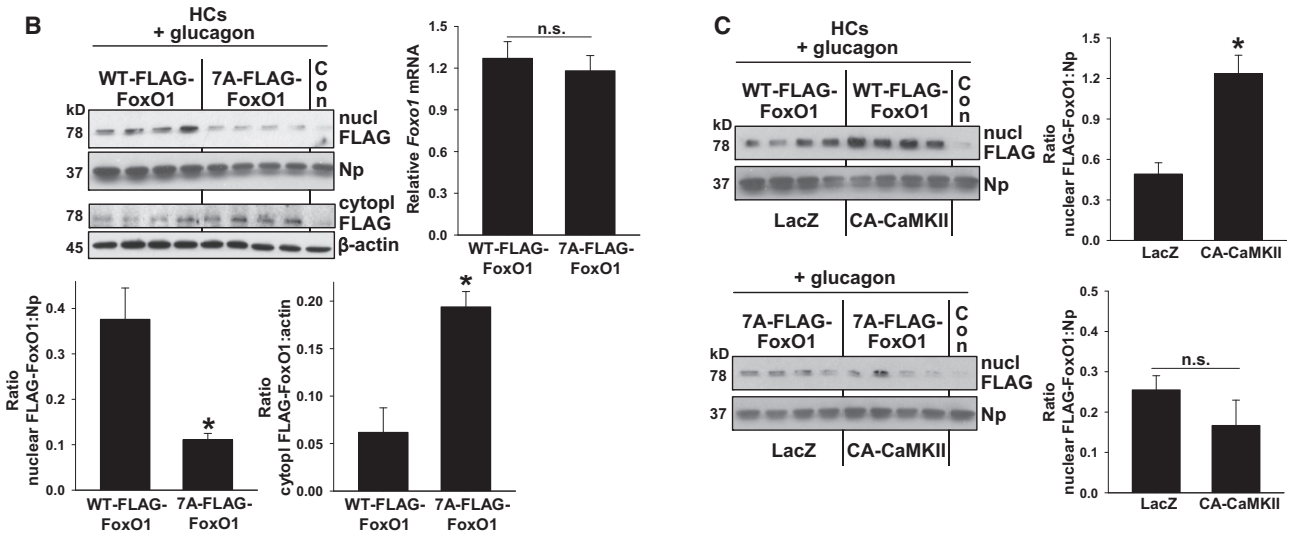

Figure 6. The Role of Non-AKT-Phospho Sites of FoxO1 in CaMKII-Mediated FoxO1 Nuclear Localization

(A) HCs from WT and *Camk2g*$^{-/-}$ mice were transduced with adeno-FLAG-FoxO1 at an MOI of 2. Cells were serum-depleted overnight and then incubated for 5 hr in serum-free media. FoxO1 was immunopurified using anti-FLAG, followed by reduction, alkylation, and proteolytic digestion. Phosphorylated peptides were enriched by TiO_2 chromatography and then analyzed by LC-MS/MS as described in Experimental Procedures. The table shows spectral count number, Debunker score, and Ascore of phosphorylated peptides in KO and WT samples; Δ in the peptide sequence indicates the phosphorylation site. The cutoff values for spectral count #, Debunker score, and Ascore are set at 5, 0.5, and 12, respectively. The spectra of peptides with scores that are below these values (italics) were checked manually to eliminate uncertain phosphorylation sites (Figures S4A and S4B for WT peptides 4 and 5; and http://fields.scripps.edu/published/foxo1_Tabas_2012/ for KO peptides 7, 10, and 11). The KO/WT ratio of spectral counts was calculated only for peptides with a combined spectral count in KO and WT >10.

(B) HCs from L-FoxO1 mice were transfected with expression plasmids encoding murine FLAG-FoxO1 or FLAG-7A-FoxO1 mutant. After 48 hr, the cells were serum-depleted overnight and then incubated with glucagon (100 nm) for 4 hr in serum-free media. Nuclear extracts were assayed by immunoblot for FLAG and nucleophosmin (nuclear loading control), and RNA from a parallel set of cells was probed for Foxo1 mRNA by RT-qPCR. Densitometric quantification of the mRNA and immunoblot data are shown in the graph (*$p \leq 0.005$; mean ± SEM).

(C) Similar to (B), except the HCs were transduced with adeno-LacZ or CA-CaMKII one day after the transfection with the WT or mutant FoxO1 plasmids (*$p = 0.003$; mean ± SEM).

phosphorylating the aforementioned Ser residues in FoxO1 (Asada et al., 2007) remains to be determined.

The Role of CaMKII in Hepatic Glucose Metabolism in Obesity

Elevated HGP, in part due to an imbalance of glucagon-to-insulin signaling, contributes to fasting hyperglycemia in obesity and other insulin-resistant states (Sørensen et al., 2006; Unger and Cherrington, 2012; Saltiel, 2001). To test the role of CaMKIIγ in hepatic glucose metabolism in the setting of obesity, we first sought evidence of hepatic CaMKIIγ activation in two mouse models of obesity. We found that the level of p-CaMKII, but not total CaMKII, was markedly higher in the livers of both *ob/ob* mice and WT mice placed on a high-fat, high-calorie diet for 20 wks (diet-induced obesity [DIO]) (Figure 7A). Antibody specificity for both anti-p-CaMKII and anti-CaMKII in obese liver is shown by the absence of the immunoblot bands in obese *Camk2g*$^{-/-}$ mice. We next tested functional importance by comparing fasting plasma glucose and hepatic FoxO1-target gene expression in *ob/ob* mice transduced with adeno-KD-CaMKII versus adeno-LacZ control. The mice treated with adeno-KD-CaMKII had lower fasting glucose, lower blood

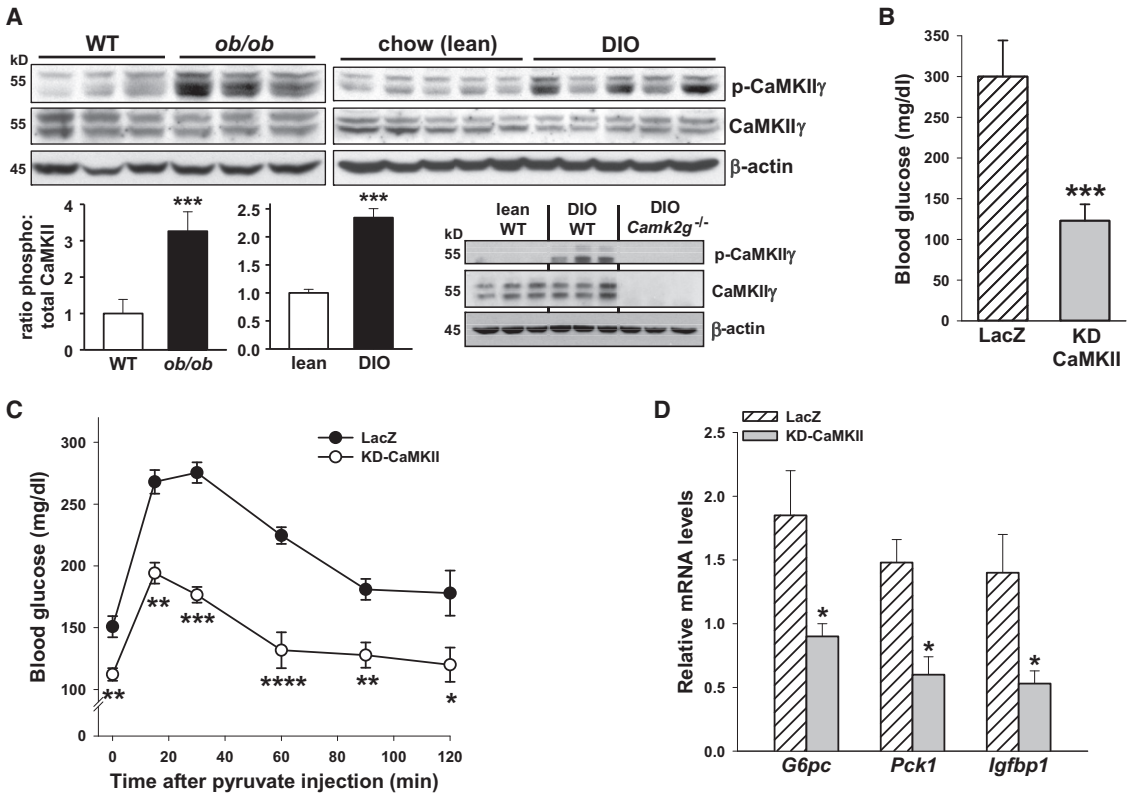

Figure 7. The Role of CaMKII in Hepatic Glucose Metabolism in Obesity

(A) Liver extracts from 10-week-old WT or *ob/ob* mice, or WT mice fed a chow or high-calorie diet for 20 wks (diet-induced obesity; DIO), were probed for phospho- and total CaMKIIγ and β-actin by immunoblot. Densitometric quantification is shown in the bar graph (***$p < 0.001$; mean ± SEM). Antibody specificity is shown by the absence of phospho- and total CaMKIIγ bands in liver extracts from DIO *Camk2g*$^{-/-}$ mice.

(B–D) Fasting blood glucose, blood glucose after pyruvate challenge, and liver *G6pc*, *Pck1*, and *Igfbp1* mRNA in *ob/ob* mice after treatment with adeno-LacZ or KD-CaMKII (n = 5/group; *$p < 0.05$, **$p < 0.01$, ***$p < 0.005$, and ****$p < 0.001$ versus LacZ; mean ± SEM). See also Figure S7.

glucose after pyruvate challenge, and lower expression of three FoxO1-target genes, including *G6pc* and *Pck1* (Figures 7B–7D) These changes were not associated with either higher plasma insulin or lower weight in the adeno-KD-CaMKII-treated mice (data not shown). Thus, hepatic CaMKII is activated in the livers of obese mice and regulates hepatic glucose metabolism and FoxO1-target gene expression.

DISCUSSION

The data in this report provide evidence for calcium-mediated regulation of HGP as part of a pathway that can be summarized as follows: glucagon/fasting → cAMP/PKA → IP3R1 → $Ca^{2+}{}_{I}$ → CaMKII → nuclear FoxO1 → HGP. CaMKII also mediates elevated HGP in obese mice (Figure 7), and although more work is needed in this area, it is possible that the driving force here is also glucagon (Sørensen et al., 2006; Unger and Cherrington, 2012; Saltiel, 2001). As such, the present findings have implications for three fundamental areas related to HGP: the molecular mechanisms whereby glucagon and fasting, as well as obesity/insulin resistance, stimulate HGP; the molecular links between intracellular calcium and HGP; and the regulation of FoxO1 nuclear transport. The latter issue is of particular interest, because while there have been many reports on how insulin/AKT-mediated phosphorylation of FoxO1, as well as FoxO1 acetylation, promote nuclear exclusion of FoxO1 (Lin and Accili, 2011; van der Horst and Burgering, 2007), there has been little emphasis on the regulation of FoxO1 nuclear *entry* that occurs in the absence of insulin or in the setting of insulin resistance.

The CaMKII pathway is downstream of cAMP/PKA, and so it would naturally complement other glucagon-PKA pathways that stimulate HGP. Thus far, our data suggest that these other pathways occur in parallel with the CaMKII pathway rather than also being downstream of CaMKII. For example, glucagon-PKA directly phosphorylates cAMP response element binding (CREB) protein, which transcriptionally induces the FoxO1 transcriptional cofactor PGC1α (Herzig et al., 2001), but there was no difference in nuclear CREB in livers from adeno-LacZ versus KD-CaMKII mice (Figure S3B). This was an important finding, because there are in vitro data in neurons and in RANKL-treated RAW264.7 cells that CaMKII can activate/phosphorylate CREB in certain settings (Dash et al., 1991; Sheng et al., 1991; Ang et al., 2007). We also found that CaMKII deficiency did not affect nuclear Crtc2 (Figure S3C), which is another transcriptional activator involved in HGP. These data indicate that CaMKII in liver works in parallel with these other pathways, which together effect the nuclear localization of the proper array of transcriptional factors to mediate HGP. The

case with Crtc2 is particularly interesting, because glucagon/PKA-mediated IP3R activation and ER calcium release promotes Crtc2 nuclear localization through another calcium-sensing enzyme, calcineurin (Wang et al., 2012). Indeed, we found that inhibition of CaMKII and calcineurin are additive in terms of suppressing forskolin-induced *G6pc* mRNA (unpublished data). Thus, a common proximal signaling pathway leads to the coordinated nuclear entry of two key HGP transcription factors, Crtc2 and FoxO1, by different distal mechanisms. In this regard, it is interesting to note a previous study showing that drugs that promote calcium entry through the plasma membrane actually decrease *Pck1* mRNA in HCs (Valera et al., 1993), which may suggest that the route of calcium entry into the cytoplasm is a factor in determining downstream events.

FoxO1 is phosphorylated at Thr24, Ser253, and Ser316 (murine sequence numbers) by insulin/growth factors via Akt to promote its nuclear exclusion. It would be counterintuitive to propose that CaMKII phosphorylates these sites, because CaMKII promotes FoxO1 nuclear localization, but CaMKII could theoretically activate a phosphatase that dephosphorylates these sites. However, CaMKIIγ deficiency did not affect the phosphorylation of these three residues, and it also did not affect FoxO1 acetylation (Figures S4A and S4B). Instead, we found evidence that CaMKII mediates the phosphorylation of other Ser residues on FoxO1, and our Ser-Ala FoxO1 mutant experiments suggest that this action plays a role in CaMKII-mediated FoxO1 nuclear localization.

The link between CaMKII and FoxO1 phosphorylation may be direct or indirect. An indirect mechanism, i.e., whereby CaMKII activates another kinase, could be linked to previous findings that other kinases can phosphorylate FoxO on non-Akt sites in a manner that promotes their nuclear retention (Essers et al., 2004; Chiacchiera and Simone, 2010). Based on the p38 inhibitor and gene-targeting data herein and the study of Asada et al. (2007), we suggest that p38 MAPK may also be able to carry out this function and, indeed, may be the mediator of CaMKII-induced FoxO1 nuclear localization. In support of this hypothesis are reports of links between CaMKII and p38 and between p38 and HGP (Cao et al., 2005; Blanquet, 2000). While there is no direct evidence yet that p38 phosphorylates and thereby activates FoxO1, the ability of glucocorticoids to promote FoxO1 nuclear localization in rat cardiomyocytes correlated with activation/phosphorylation of nuclear p38, and immunofluorescence microscopy and IP/immunoblot data suggested that phospho-p38 and FoxO1 may interact with each other (Puthanveetil et al., 2010). Interestingly, there is evidence that FoxO1 may be able to activate p38 in HCs (Naïmi et al., 2007), and so it is possible that a FoxO1-p38 feed-forward pathway might amplify the effect the CaMKII-p38 pathway suggested here on FoxO1 nuclear localization. However, more work is needed to establish the role of p38 and to further elucidate the mechanisms whereby CaMKII promotes FoxO1 nuclear localization.

The discovery of the role of calcium-CaMKII in HGP not only provides insight into the physiologic defense against fasting hypoglycemia but may also reveal therapeutic targets for the disturbed glucose metabolism that occurs in the setting of insulin resistance, as suggested by the data in Figure 7. Indeed, in type 2 diabetes, disproportionate HGP and an imbalance of glucagon versus insulin signaling contributes to fasting hyperglycemia (Sørensen et al., 2006; Saltiel, 2001). Moreover, glucagon signaling has also been implicated in type 1 diabetes (Unger and Cherrington, 2012). In this context, future studies will further address the pathophysiologic role(s) and mechanisms of hepatic CaMKIIγ in obesity, insulin resistance, and diabetes and thereby evaluate its potential as a therapeutic target in these disorders.

EXPERIMENTAL PROCEDURES

Measurement of CaMKII Activity

CaMKII activity was assayed using a CaMKII assay kit from Promega according to the manufacturer's instructions. After the HCs were treated as indicated in the figure legends, they were lysed by a 5 min exposure to 1% Triton X-100 in 50 mM HEPES, 150 mM NaCl, 10 mM Na pyrophosphate, 10 mM EDTA, 10 mM EGTA, 1 mM Na_3VO_4, 50 mM NaF, 1 mM phenylmethylsulfonyl fluoride, and 5 μg ml^{-1} leupeptin. Next, [γ-^{32}P]ATP and biotinylated CaMKII peptide substrate were added to the lysate or to the immunoprecipitated complexes (see below). After incubation for 10 min at 30°C, the [^{32}P]-phosphorylated substrate was separated from the residual [^{32}P]ATP using SAM biotin-capture membrane and then quantitated using a scintillation counter. Assays were conducted with or without calmodulin, and the activity value in the absence of calmodulin was subtracted from those obtained in the presence of calmodulin.

Glucose Production in Primary HCs

Glucose production assays were carried out as described (Yoon et al., 2001). Briefly, after primary mouse HCs were harvested and cultured as described above, the cell culture medium was switched to glucose- and phenol-free DMEM (pH 7.4) supplemented with 20 mM sodium lactate and 2 mM sodium pyruvate. After 16 hr of culture, 500 μl medium was collected, and the glucose content was measured using a colorimetric glucose assay kit (Abcam). The readings were then normalized to the total protein amount in the whole-cell lysates.

Mouse Experiments

Camk2g$^{-/-}$ mice were generated as described previously (Backs et al., 2010) and crossed onto the C57BL6/J background. *ob/ob* mice were obtained from Jackson Labs. Mice were fed a standard chow diet, or a high-fat diet with 60% kcal from fat for the experiments in Figure 7, and maintained on a 12-hr-light-dark cycle. Recombinant adenovirus (1.5×10^9 plaque-forming unit/mice) was delivered by tail vein injection, and experiments were commenced after 5 days. Fasting blood glucose was measured in mice that were fasted for 12–14 hr, with free access to water, using a glucose meter (One Touch Ultra, Lifescan). Pyruvate-tolerance tests were carried out with an intraperitoneal injection of 2 g kg^{-1} body weight pyruvate after 17 hr of fasting. Blood glucose levels were measured over the following 2 hr. Xestospongin C was administered by daily i.p. injections to mice at a dose of 10 pmol g^{-1} for 4 days. *P38a*$^{fl/fl}$ mice were generated as described previously (Engel et al., 2005) and generously provided by Dr. Yibin Wang, UCLA School of Medicine. Animal studies were performed in accordance with the Columbia University Animal Research Committee.

Hepatic Glycogen Measurement

Frozen livers (50–100 mg) were homogenized in 1 ml of H_2O with protease and phosphatase inhibitors. Samples were then mixed with KOH (1:2), boiled for 25 min and washed with 70% ethanol. The pellet was dried and dissolved in 100 μl H_2O, and the glycogen content was assessed using the Glycogen Assay Kit (Abcam) according to the manufacturer's instructions. Data represent the mean ± SEM.

PAS Staining of Mouse Liver Sections

Liver samples were fixed in 10% neutral-buffered formalin for 24 hr and embedded in paraffin. Sections (5 μm) were stained for glycogen using PAS stain (Sigma) according to manufacturer's instructions. The sections were then counterstained with hematoxylin and examined by light microscopy. For the quantification of PAS staining, five fields from four different sections were chosen randomly, and the number of PAS-positive cells was counted and expressed as the percentage of the total number of cells (Hammad et al., 1982). Two independent investigators, blinded to the identity of the samples, performed the analysis.

Analysis of Mass Spectrometric Data

Protein and phosphopeptide identification, quantification, and phospho analysis were performed with Integrated Proteomics Pipeline - IP2 (Integrated Proteomics Applications, Inc., San Diego, CA. http://www.integratedproteomics.com/) using ProLuCID, DTASelect2, Census, DeBunker, and Ascore. Spectrum raw files were extracted into ms1 and ms2 files (McDonald et al., 2004) from raw files using RawExtract 1.9.9 (http://fields.scripps.edu/downloads.php) and the tandem mass spectra were searched against EBI IPI mouse protein database (http://www.ebi.ac.uk/IPI/IPImouse.html, released on March 24, 2010). In order to accurately estimate peptide probabilities and FDRs, we used a decoy database containing the reversed sequences of all the proteins appended to the target database (Peng et al., 2003). Tandem mass spectra were matched to sequences using the ProLuCID (Xu et al., 2006) algorithm with 50 ppm peptide mass tolerance. ProLuCID searches were done on an Intel Xeon cluster running under the Linux operating system. The search space included all fully and half-tryptic peptide candidates that fell within the mass tolerance window. Carbamidomethylation (+57.02146 Da) of cysteine was considered as a static modification, while phosphorylation (+79.9663) on serine, threonine, and tyrosine were considered as variable modifications.

The validity of peptide/spectrum matches (PSMs) was assessed in DTASelect (Tabb et al., 2002; Cociorva et al., 2007) using two SEQUEST (Eng et al., 1994) defined parameters, the cross-correlation score (XCorr), and normalized difference in cross-correlation scores (DeltaCN). The search results were grouped by charge state (+1, +2, +3, and greater than +3) and tryptic status (fully tryptic, half-tryptic, and nontryptic), resulting in 12 distinct subgroups. In each one of these subgroups, the distribution of Xcorr, DeltaCN, and DeltaMass values for (1) direct and (2) decoy database PSMs was obtained, and then the direct and decoy subsets were separated by discriminant analysis. Full separation of the direct and decoy PSM subsets is not generally possible; therefore, peptide match probabilities were calculated based on a nonparametric fit of the direct and decoy score distributions. A peptide confidence of 99.5% was set as the minimum threshold, and only phosphopeptides with delta mass less than 10 ppm were accepted. The FDR was calculated as the percentage of reverse decoy PSMs among all the PSMs that passed the 99.5% confidence threshold. After this last filtering step, we estimate that both the protein and peptide FDRs were both below 0.1%. After database searching and DTASelect2 filtering, phosphopeptides were analyzed with IP2 phospho analysis tool that uses Ascore (Beausoleil et al., 2006) and Debunker (Lu et al., 2007). Peptides and phosphopeptides were quantified using the Spectral Count method (Liu et al., 2004).

Statistical Analysis

All results are presented as mean ± SEM. p values were calculated using the Student's t test for normally distributed data and the Mann-Whitney rank sum test for nonnormally distributed data.

SUPPLEMENTAL INFORMATION

Supplemental Information includes five figures, Supplemental Experimental Procedures, and two tables and can be found with this article online at doi:10.1016/j.cmet.2012.03.002.

ACKNOWLEDGMENTS

We thank Dr. Eric Olson (University of Texas Southwestern Medical Center) for the *Camk2g*$^{-/-}$ mice and Dr. Marc Montminy (Salk Institute for Biological Sciences) for anti-Crtc2 antibody. This work was supported by an American Heart Association Scientist Development Grant to L.O.; Emmy Noether-DFG grant 2258/2-1 to J.B.; NIH grant P41 RR011823 to C.C.L.W. and J.Y.; and NHLBI Proteomic Centers grants HHSN268201000035C to T.X., HL49426 to H.A.S., HL087123 and DK057539 to D.A., and HL087123 and HL075662 to I.T.

Received: August 14, 2011
Revised: January 20, 2012
Accepted: March 5, 2012
Published online: April 12, 2012

REFERENCES

Accili, D., and Arden, K.C. (2004). FoxOs at the crossroads of cellular metabolism, differentiation, and transformation. Cell *117*, 421–426.

Ang, E.S., Zhang, P., Steer, J.H., Tan, J.W., Yip, K., Zheng, M.H., Joyce, D.A., and Xu, J. (2007). Calcium/calmodulin-dependent kinase activity is required for efficient induction of osteoclast differentiation and bone resorption by receptor activator of nuclear factor kappa B ligand (RANKL). J. Cell. Physiol. *212*, 787–795.

Asada, S., Daitoku, H., Matsuzaki, H., Saito, T., Sudo, T., Mukai, H., Iwashita, S., Kako, K., Kishi, T., Kasuya, Y., and Fukamizu, A. (2007). Mitogen-activated protein kinases, Erk and p38, phosphorylate and regulate Foxo1. Cell. Signal. *19*, 519–527.

Ayala, J.E., Streeper, R.S., Desgrosellier, J.S., Durham, S.K., Suwanichkul, A., Svitek, C.A., Goldman, J.K., Barr, F.G., Powell, D.R., and O'Brien, R.M. (1999). Conservation of an insulin response unit between mouse and human glucose-6-phosphatase catalytic subunit gene promoters: transcription factor FKHR binds the insulin response sequence. Diabetes *48*, 1885–1889.

Backs, J., Stein, P., Backs, T., Duncan, F.E., Grueter, C.E., McAnally, J., Qi, X., Schultz, R.M., and Olson, E.N. (2010). The gamma isoform of CaM kinase II controls mouse egg activation by regulating cell cycle resumption. Proc. Natl. Acad. Sci. USA *107*, 81–86.

Barthel, A., Schmoll, D., Krüger, K.D., Bahrenberg, G., Walther, R., Roth, R.A., and Joost, H.G. (2001). Differential regulation of endogenous glucose-6-phosphatase and phosphoenolpyruvate carboxykinase gene expression by the forkhead transcription factor FKHR in H4IIE-hepatoma cells. Biochem. Biophys. Res. Commun. *285*, 897–902.

Beausoleil, S.A., Villén, J., Gerber, S.A., Rush, J., and Gygi, S.P. (2006). A probability-based approach for high-throughput protein phosphorylation analysis and site localization. Nat. Biotechnol. *24*, 1285–1292.

Blanquet, P.R. (2000). Identification of two persistently activated neurotrophin-regulated pathways in rat hippocampus. Neuroscience *95*, 705–719.

Brunet, A., Bonni, A., Zigmond, M.J., Lin, M.Z., Juo, P., Hu, L.S., Anderson, M.J., Arden, K.C., Blenis, J., and Greenberg, M.E. (1999). Akt promotes cell survival by phosphorylating and inhibiting a Forkhead transcription factor. Cell *96*, 857–868.

Burgess, S.C., He, T., Yan, Z., Lindner, J., Sherry, A.D., Malloy, C.R., Browning, J.D., and Magnuson, M.A. (2007). Cytosolic phosphoenolpyruvate carboxykinase does not solely control the rate of hepatic gluconeogenesis in the intact mouse liver. Cell Metab. *5*, 313–320.

Bygrave, F.L., and Benedetti, A. (1993). Calcium: its modulation in liver by cross-talk between the actions of glucagon and calcium-mobilizing agonists. Biochem. J. *296*, 1–14.

Cantin, G.T., Shock, T.R., Park, S.K., Madhani, H.D., and Yates, J.R., 3rd. (2007). Optimizing TiO2-based phosphopeptide enrichment for automated multidimensional liquid chromatography coupled to tandem mass spectrometry. Anal. Chem. *79*, 4666–4673.

Cao, W., Collins, Q.F., Becker, T.C., Robidoux, J., Lupo, E.G., Jr., Xiong, Y., Daniel, K.W., Floering, L., and Collins, S. (2005). p38 Mitogen-activated protein kinase plays a stimulatory role in hepatic gluconeogenesis. J. Biol. Chem. *280*, 42731–42737.

Chiacchiera, F., and Simone, C. (2010). The AMPK-FoxO3A axis as a target for cancer treatment. Cell Cycle *9*, 1091–1096.

Cociorva, D., Tabb, L., and Yates, J.R. (2007). Validation of tandem mass spectrometry database search results using DTASelect. Curr. Protoc. Bioinformatics., *Chapter 13:Unit 13.4*.

Couchonnal, L.F., and Anderson, M.E. (2008). The role of calmodulin kinase II in myocardial physiology and disease. Physiology *23*, 151–159.

Dash, P.K., Karl, K.A., Colicos, M.A., Prywes, R., and Kandel, E.R. (1991). cAMP response element-binding protein is activated by Ca2+/calmodulin- as well as cAMP-dependent protein kinase. Proc. Natl. Acad. Sci. USA *88*, 5061–5065.

Eng, J.K., McCormack, A.L., and Yates, J.R., III. (1994). An approach to correlate tandem mass spectral data of peptides with amino acid sequences in a protein database. J. Am. Soc. Mass Spectrom. *5*, 976–989.

Engel, F.B., Schebesta, M., Duong, M.T., Lu, G., Ren, S., Madwed, J.B., Jiang, H., Wang, Y., and Keating, M.T. (2005). p38 MAP kinase inhibition enables proliferation of adult mammalian cardiomyocytes. Genes Dev. *19*, 1175–1187.

Essers, M.A., Weijzen, S., de Vries-Smits, A.M., Saarloos, I., de Ruiter, N.D., Bos, J.L., and Burgering, B.M. (2004). FOXO transcription factor activation by oxidative stress mediated by the small GTPase Ral and JNK. EMBO J. *23*, 4802–4812.

Friedmann, N., and Rasmussen, H. (1970). Calcium, manganese and hepatic gluconeogenesis. Biochim. Biophys. Acta *222*, 41–52.

Hall, R.K., Sladek, F.M., and Granner, D.K. (1995). The orphan receptors COUP-TF and HNF-4 serve as accessory factors required for induction of phosphoenolpyruvate carboxykinase gene transcription by glucocorticoids. Proc. Natl. Acad. Sci. USA *92*, 412–416.

Hammad, E.S., Striffler, J.S., and Cardell, R.R., Jr. (1982). Morphological and biochemical observations on hepatic glycogen metabolism in genetically diabetic (db/db) mice. Diabete Metab. *8*, 147–153.

Hansen, L.H., Gromada, J., Bouchelouche, P., Whitmore, T., Jelinek, L., Kindsvogel, W., and Nishimura, E. (1998). Glucagon-mediated Ca2+ signaling in BHK cells expressing cloned human glucagon receptors. Am. J. Physiol. *274*, C1552–C1562.

Harano, Y., Kashiwagi, A., Kojima, H., Suzuki, M., Hashimoto, T., and Shigeta, Y. (1985). Phosphorylation of carnitine palmitoyltransferase and activation by glucagon in isolated rat hepatocytes. FEBS Lett. *188*, 267–272.

Herzig, S., Long, F., Jhala, U.S., Hedrick, S., Quinn, R., Bauer, A., Rudolph, D., Schutz, G., Yoon, C., Puigserver, P., et al. (2001). CREB regulates hepatic gluconeogenesis through the coactivator PGC-1. Nature *413*, 179–183.

Kraus-Friedmann, N., and Feng, L. (1996). The role of intracellular Ca2+ in the regulation of gluconeogenesis. Metabolism *45*, 389–403.

Lin, H.V., and Accili, D. (2011). Hormonal regulation of hepatic glucose production in health and disease. Cell Metab. *14*, 9–19.

Liu, H., Sadygov, R.G., and Yates, J.R., 3rd. (2004). A model for random sampling and estimation of relative protein abundance in shotgun proteomics. Anal. Chem. *76*, 4193–4201.

Lu, B., Ruse, C., Xu, T., Park, S.K., and Yates, J., 3rd. (2007). Automatic validation of phosphopeptide identifications from tandem mass spectra. Anal. Chem. *79*, 1301–1310.

MacCoss, M.J., McDonald, W.H., Saraf, A., Sadygov, R., Clark, J.M., Tasto, J.J., Gould, K.L., Wolters, D., Washburn, M., Weiss, A., et al. (2002). Shotgun identification of protein modifications from protein complexes and lens tissue. Proc. Natl. Acad. Sci. USA *99*, 7900–7905.

Marques-da-Silva, A.C., D'Avila, R.B., Ferrari, A.G., Kelmer-Bracht, A.M., Constantin, J., Yamamoto, N.S., and Bracht, A. (1997). Ca2+ dependence of gluconeogenesis stimulation by glucagon at different cytosolic NAD(+)-NADH redox potentials. Braz. J. Med. Biol. Res. *30*, 827–836.

Matsumoto, M., Pocai, A., Rossetti, L., Depinho, R.A., and Accili, D. (2007). Impaired regulation of hepatic glucose production in mice lacking the forkhead transcription factor Foxo1 in liver. Cell Metab. *6*, 208–216.

McDonald, W.H., Tabb, D.L., Sadygov, R.G., MacCoss, M.J., Venable, J., Graumann, J., Johnson, J.R., Cociorva, D., and Yates, J.R., 3rd. (2004). MS1, MS2, and SQT-three unified, compact, and easily parsed file formats for the storage of shotgun proteomic spectra and identifications. Rapid Commun. Mass Spectrom. *18*, 2162–2168.

Mine, T., Kojima, I., and Ogata, E. (1993). Role of calcium fluxes in the action of glucagon on glucose metabolism in rat hepatocytes. Am. J. Physiol. *265*, G35–G42.

Naïmi, M., Gautier, N., Chaussade, C., Valverde, A.M., Accili, D., and Van Obberghen, E. (2007). Nuclear forkhead box O1 controls and integrates key signaling pathways in hepatocytes. Endocrinology *148*, 2424–2434.

Nakae, J., Kitamura, T., Silver, D.L., and Accili, D. (2001). The forkhead transcription factor Foxo1 (Fkhr) confers insulin sensitivity onto glucose-6-phosphatase expression. J. Clin. Invest. *108*, 1359–1367.

Nakae, J., Biggs, W.H., 3rd, Kitamura, T., Cavenee, W.K., Wright, C.V., Arden, K.C., and Accili, D. (2002). Regulation of insulin action and pancreatic beta-cell function by mutated alleles of the gene encoding forkhead transcription factor Foxo1. Nat. Genet. *32*, 245–253.

Peng, J., Elias, J.E., Thoreen, C.C., Licklider, L.J., and Gygi, S.P. (2003). Evaluation of multidimensional chromatography coupled with tandem mass spectrometry (LC/LC-MS/MS) for large-scale protein analysis: the yeast proteome. J. Proteome Res. *2*, 43–50.

Pfleiderer, P.J., Lu, K.K., Crow, M.T., Keller, R.S., and Singer, H.A. (2004). Modulation of vascular smooth muscle cell migration by calcium/calmodulin-dependent protein kinase II-delta 2. Am. J. Physiol. Cell Physiol. *286*, C1238–C1245.

Pilkis, S.J., and Granner, D.K. (1992). Molecular physiology of the regulation of hepatic gluconeogenesis and glycolysis. Annu. Rev. Physiol. *54*, 885–909.

Puigserver, P., Rhee, J., Donovan, J., Walkey, C.J., Yoon, J.C., Oriente, F., Kitamura, Y., Altomonte, J., Dong, H., Accili, D., and Spiegelman, B.M. (2003). Insulin-regulated hepatic gluconeogenesis through FOXO1-PGC-1alpha interaction. Nature *423*, 550–555.

Puthanveetil, P., Wang, Y., Wang, F., Kim, M.S., Abrahani, A., and Rodrigues, B. (2010). The increase in cardiac pyruvate dehydrogenase kinase-4 after short-term dexamethasone is controlled by an Akt-p38-forkhead box other factor-1 signaling axis. Endocrinology *151*, 2306–2318.

Radziuk, J., and Pye, S. (2001). Hepatic glucose uptake, gluconeogenesis and the regulation of glycogen synthesis. Diabetes Metab. Res. Rev. *17*, 250–272.

Rhee, J., Inoue, Y., Yoon, J.C., Puigserver, P., Fan, M., Gonzalez, F.J., and Spiegelman, B.M. (2003). Regulation of hepatic fasting response by PPARgamma coactivator-1alpha (PGC-1): requirement for hepatocyte nuclear factor 4alpha in gluconeogenesis. Proc. Natl. Acad. Sci. USA *100*, 4012–4017.

Saltiel, A.R. (2001). New perspectives into the molecular pathogenesis and treatment of type 2 diabetes. Cell *104*, 517–529.

Sheng, M., Thompson, M.A., and Greenberg, M.E. (1991). CREB: a Ca(2+)-regulated transcription factor phosphorylated by calmodulin-dependent kinases. Science *252*, 1427–1430.

Singer, H.A. (2011). Ca2+/calmodulin-dependent protein kinase II Function in vascular remodeling. J. Physiol. Published online November 28, 2011. 10.1113/jphysiol.2011.222232.

Sørensen, H., Brand, C.L., Neschen, S., Holst, J.J., Fosgerau, K., Nishimura, E., and Shulman, G.I. (2006). Immunoneutralization of endogenous glucagon reduces hepatic glucose output and improves long-term glycemic control in diabetic ob/ob mice. Diabetes *55*, 2843–2848.

Staddon, J.M., and Hansford, R.G. (1989). Evidence indicating that the glucagon-induced increase in cytoplasmic free Ca2+ concentration in hepatocytes is mediated by an increase in cyclic AMP concentration. Eur. J. Biochem. *179*, 47–52.

Tabb, D.L., McDonald, W.H., and Yates, J.R., 3rd. (2002). DTASelect and Contrast: tools for assembling and comparing protein identifications from shotgun proteomics. J. Proteome Res. *1*, 21–26.

Unger, R.H., and Cherrington, A.D. (2012). Glucagonocentric restructuring of diabetes: a pathophysiologic and therapeutic makeover. J. Clin. Invest. *122*, 4–12.

Valera, A., Solanes, G., and Bosch, F. (1993). Calcium-mobilizing effectors inhibit P-enolpyruvate carboxykinase gene expression in cultured rat hepatocytes. FEBS Lett. *333*, 319–324.

van der Horst, A., and Burgering, B.M. (2007). Stressing the role of FoxO proteins in lifespan and disease. Nat. Rev. Mol. Cell Biol. *8*, 440–450.

von Groote-Bidlingmaier, F., Schmoll, D., Orth, H.M., Joost, H.G., Becker, W., and Barthel, A. (2003). DYRK1 is a co-activator of FKHR (FOXO1a)-dependent glucose-6-phosphatase gene expression. Biochem. Biophys. Res. Commun. *300*, 764–769.

Wang, Y., Li, G., Goode, J., Paz, J.C., Screaton, R., Fischer, W.H., Tabas, I., and Montminy, M. (2012). Inositol 1,4,5-trisphosphate receptor regulates fasting hepatic gluconeogenesis. Nature, in press.

Xu, T., Venable, J.D., Park, S.K., Cociorva, D., Lu, B., Liao, L., Wohlschlegel, J., Hewel, J., and Yates, J.R. (2006). ProLuCID, a fast and senstive tandem mass spectra-based protein identification program. Mol. Cell. Proteomics *5*, S174.

Yoon, J.C., Puigserver, P., Chen, G., Donovan, J., Wu, Z., Rhee, J., Adelmant, G., Stafford, J., Kahn, C.R., Granner, D.K., et al. (2001). Control of hepatic gluconeogenesis through the transcriptional coactivator PGC-1. Nature *413*, 131–138.

Cell Metabolism, Volume *15*

Supplemental Information

Calcium Signaling through CaMKII Regulates Hepatic Glucose Production in Fasting and Obesity

Lale Ozcan, Catherine C.L. Wong, Gang Li, Tao Xu, Utpal Pajvani, Sung Kyu Robin Park, Anetta Wronska, Bi-Xing Chen, Andrew R. Marks, Akiyoshi Fukamizu, Johannes Backs, Harold A. Singer, John R. Yates, III, Domenico Accili, and Ira Tabas

The website at http://fields.scripps.edu/published/foxo1_Tabas_2012/) includes raw mass spectrometry data and parameter files and annotated tandem mass spectra for WT peptides 7, 10, and 11 (3 figures in supple_S1.pptx).

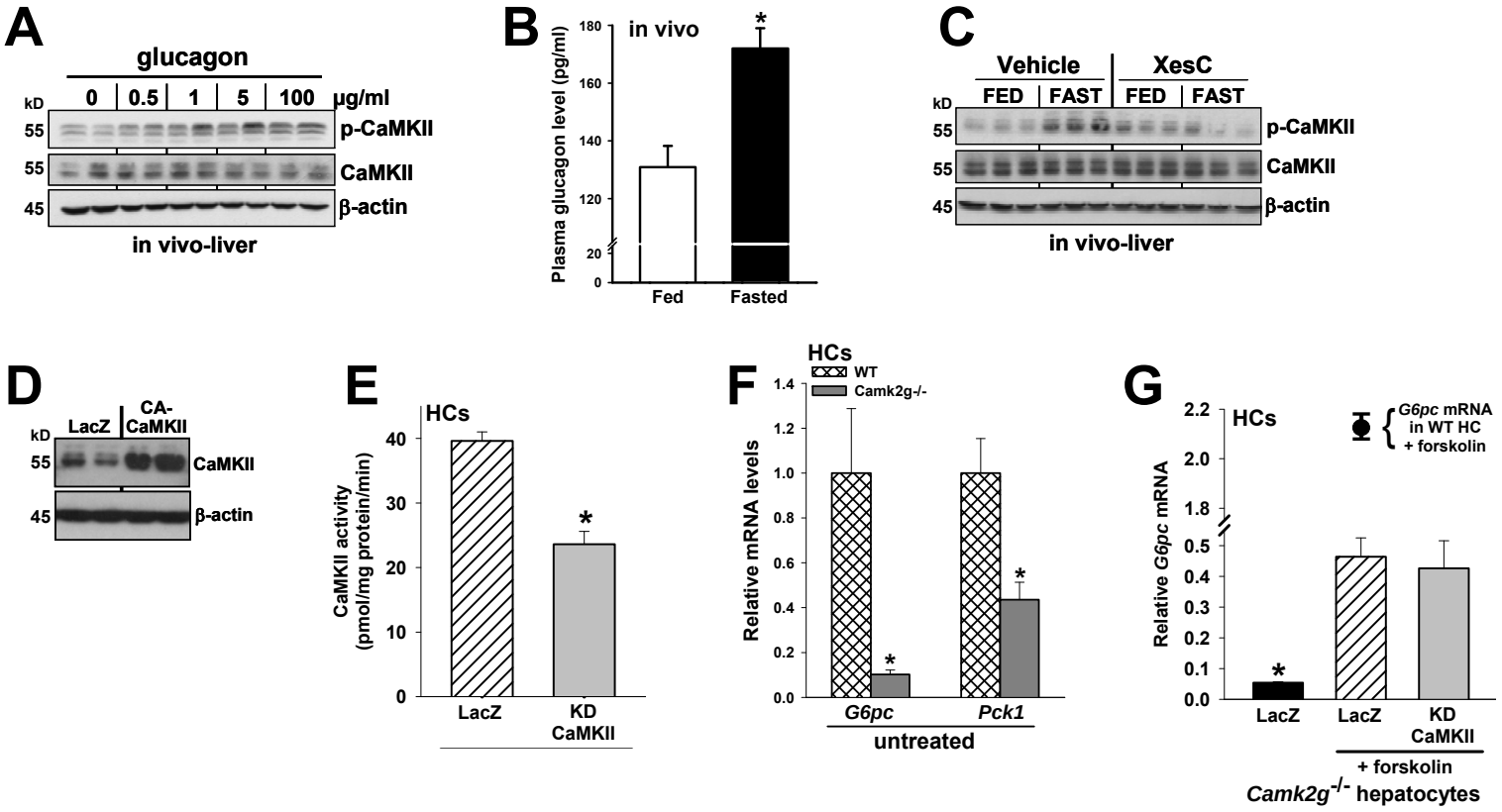

Figure S1. Related to Figures 1-2

(A) Mice were injected i.p. with the indicated doses of glucagon and sacrificed 15 min later. The livers were probed for phospho- and total CaMKII and β-actin by immunoblot.

(B) Mice (n= 5/group) were fed ad libitum or fasted for 12 h and then plasma was assayed for glucagon (*P = 0.007; mean ± S.E.M.).

(C) Mice were injected i.p. with 10 pmol g^{-1} xestospongin C (XesC) or vehicle control each day for 4 days and then fed ad libitum or fasted for 12 h. Liver phospho-CaMKII, total CaMKII, and β-actin levels were assayed by immunoblot.

(D) Immunoblot of CaMKII in HCs transduced with adeno-LacZ vs. CA-CaMKII.

(E) HCs were transduced with adeno-LacZ or KD-CaMKII. Cells were serum-depleted overnight and then assayed for CaMKII activity (*P < 0.005; mean ± S.E.M.).

(F) *G6pc* and *Pck1* mRNA levels in untreated HCs from WT vs. *Camk2g*$^{-/-}$ mice (*P 0.05). In comparison to the mRNA levels in forskolin-treated WT HCs in Figure 2D, the levels of *G6pc* and *Pck1* in untreated WT HCs was ~165-fold and ~2500-fold lower, respectively.

(G) HCs from *Camk2g*$^{-/-}$ mice were transduced with adeno-LacZ or KD-CaMKII as in (D), incubated for 14 h in media ± forskolin, and then assayed for *G6pc* mRNA (*P < 0.05 vs. the other 2 groups; mean ± S.E.M.). The black circle represents the *G6pc* mRNA value for forskolin-treated, adeno-LacZ WT HCs (1.99 ± 0.3; *P < 0.001 vs. *Camk2g*$^{-/-}$ value; mean ± S.E.M.).

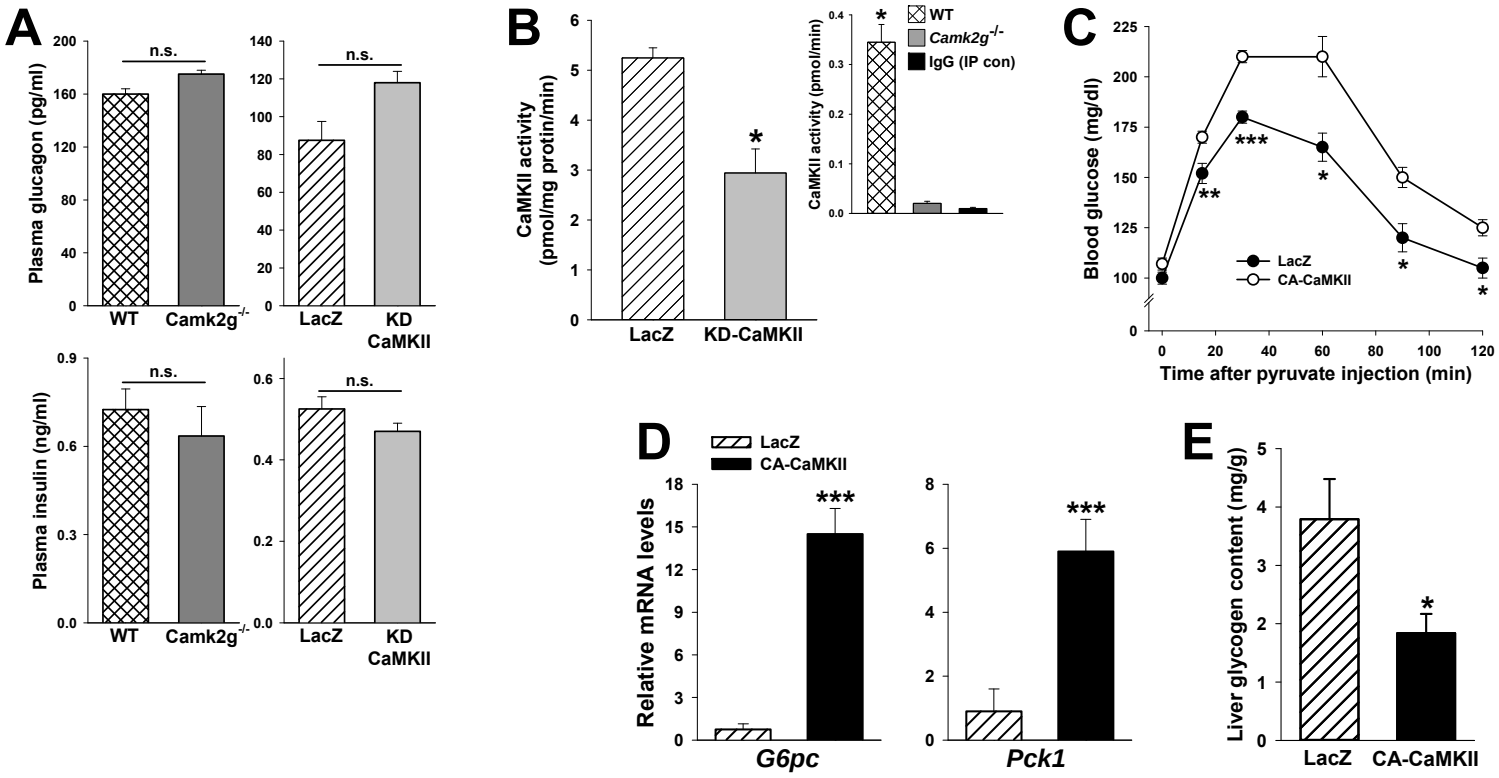

Figure S2. Related to Figure 3

(A) Fasting glucagon and insulin levels were assayed in the plasma of WT and *Camk2g*$^{-/-}$ mice and in WT mice treated with adeno-LacZ or KD-CaMKII (n = 5/group); n.s., non-significant.

(B) CaMKII was immunoprecipitated (IP) from the livers of mice treated with adeno-LacZ or KD-CaMKII and then assayed for CaMKII activity. The data in the inset validates the CaMKII assay by showing that kinase activity was negligible in the livers of *Camk2g*$^{-/-}$ mice and when non-immune IgG was used in the CaMKII IP part of the protocol (*P < 0.006; mean ± S.E.M.).

(C-D) WT mice were treated with adeno-LacZ or CA-CaMKII (n = 5/group). After 5 days, the mice were assayed for blood glucose before or after pyruvate challenge, and then, after a period of ad libitum feeding, the mice were sacrificed, and the livers were assayed for *G6pc* and *Pck1* mRNA (*P < 0.05; **P < 0.01; ***, P < 0.005; mean ± S.E.M.).

(E) Mice were treated with adeno-LacZ or CA-CaMKII (n = 5/group). After 5 days, the mice were fasted overnight and then the livers were assayed for glycogen content (*P < 0.05; mean ± S.E.M.).

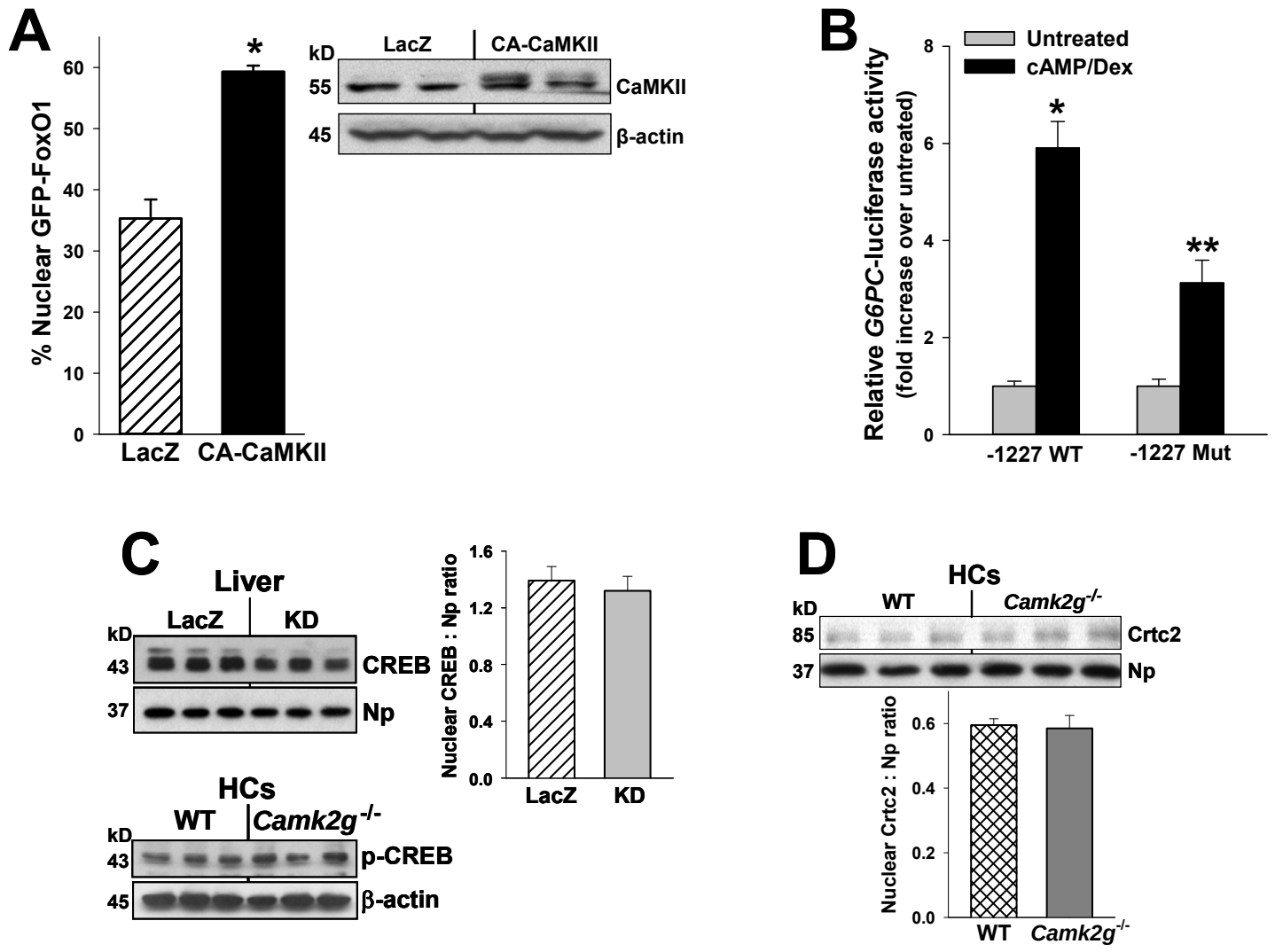

Figure S3. Related to Figures 4-5

(A) HCs were transduced with adeno-LacZ or CA-CaMKII at an MOI of 1 and transduced 4h later with adeno-GFP-FoxO1. After incubation in serum-depleted medium o.n. and then serum-free medium for 5 h, the cells were treated with 100 nM insulin for 15 min. FoxO1 subcellular localization was quantified. (*P < 0.005; mean ± S.E.M.). *Inset*, the lysate from a parallel set of cells were probed for CaMKII and β-actin by immunoblot.

(B) FAO hepatocytes were transfected with luciferase fusion constructs encoding nucleotides -1227 to +57 of the G6PC promoter containing either intact (-1227 WT) or mutated FoxO binding sites (-1227 Mut). Relative luciferase activity was measured following a 16-h incubation in the absence or presence of 0.1 mM cAMP and 1 μM dexamethasone. *P < 0.001 vs. all other groups; **P = 0.009 vs. untreated Mut (mean ± S.E.M.).

(C) Nuclei from the livers of the adeno-LacZ and KD-CaMKII-treated mice were probed by immunoblot for CREB or Crtc2 and nucleophosmin (Np), and cell extracts of glucagon-treated HCs from WT or *Camk2g*$^{-/-}$ mice were probed for p-CREB and β-actin.

(D) Nuclei from glucagon-treated HCs from WT or *Camk2g*$^{-/-}$ mice were probed for Crtc2 and nucleophosmin (Np).

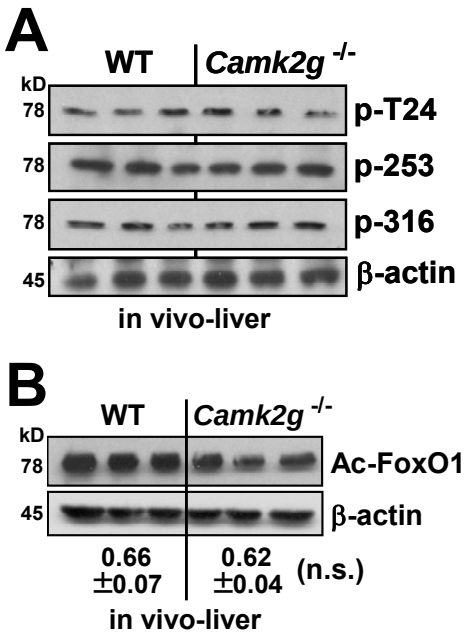

C

1 maeapqvvet dpdfeplprq rsc**T**[24]wplprp efnqsnstts
41 spapsggaaa npdaaaslas asavstdfms nlslleesed
81 farapgcvav aaaaaasrgl cgdfqgpeag cvhpappqpp
121 ptgplsqppp vppsaaaaag plagqprkts ssrrnawgnl
161 syadlitkai essaekrltl sqiyewmvks vpyfkdkgds
201 nssagwknsi rhnlslhskf irvqnegtgk sswwmlnpeg
241 gksgk**S**[246]prrr aa**S**[253]mdnnskf aksrgraakk kaslqsgqeg
281 pgd**S**[284]pgsqfs kwpa**S**[295]pgshs nddfdnwstf rprtssnast
321 isgrl**S**[326]pimt eqddlgdgdv hslvyppsaa kmastlpsls
361 eisnpenmen lldnlnllss ptsltvstqs spgsmmqqtp cysfappnts
411 ln**S**[413]p**S**[415]pnysk ytygqssmsp lpqmpmqtlq dskssyggln
451 qyncapgllk elltsd**S**[467]pph ndim**S**[475]pvdpg vaqpnsrvlg
491 qnvmmgpnsv mpaygsqash nkmmnpssht hpghaqqtas
531 vngrtlphvv ntmphtsamn rl**T**[553]pvktplq vplshpmqms
571 algsyssvss cngygrmgvl hqeklpsdld gmfierldcd
611 mesiirndlm dgdtldfnfd nvlpnqsfph svkttthswv sg

(amino acids whose phospho sites were identified by MS/MS using stringent selection criteria are in bold font—see Fig. 6A)

- Lower phospho in KO: **S295**, **467**, **475** (S246 showed lower trend in KO but spectral count not >10)
- Higher phospho in KO: **S326**
- Possible sites phosphorylated by p38 according to Asada *et al*., Cellular Signalling, 19:519 (2007): **Ser284, 295, 467, and 475**
- S-A residues in 7A-FoxO1: **S246**, **284**, **295**, **413**, **415**, **429**, **475**
- Additional S-A residues in 9A-FoxO1: **S326**, **467**

Figure S4. Related to Figure 6. FoxO1 Phosphorylation
(A) Extracts of liver from fasted WT and *Camk2g*$^{-/-}$ mice were immunoblotted for phospho-T24-, 253-, and 316-FoxO1 and β-actin.
(B) Extracts of liver from fasted adeno-FoxO1-treated WT and *Camk2g*$^{-/-}$ mice immunoblotted for acetylated FoxO1 (Ac-FoxO1) and β-actin. Average Ac-FoxO:β-actin densitometric ratio values appear below the blot; n.s., non-significant.
(C) Murine FoxO1 sequence, with identified phospho-sites in bold font; summary of data for key residues relevant to Figs. 6, S4F, and S5 are shown below in the bullet list below the sequence.

D

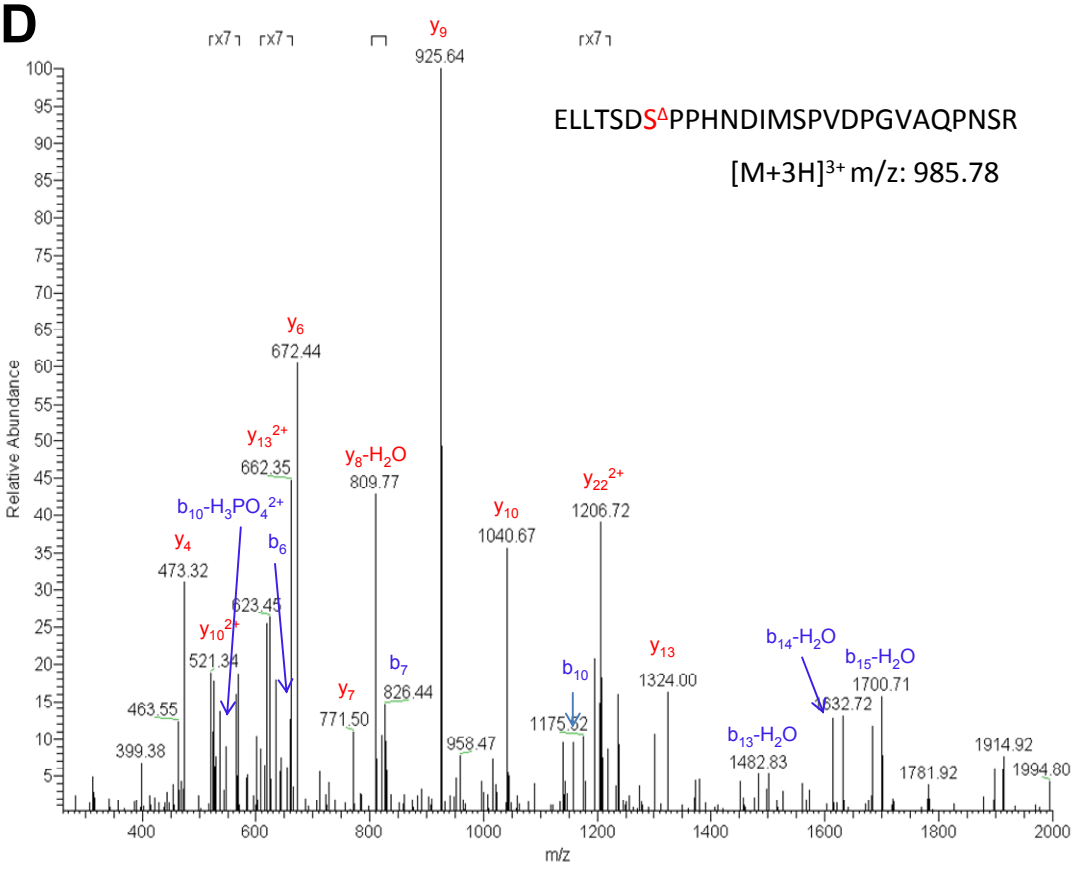

b+	b2+	#	Seq	#	y+	y2+
130.0499	65.5286	1	E	27		
243.1339	122.0706	2	L	26	2824.2971	1412.6522
356.2180	178.6126	3	L	25	2711.2131	1356.1102
457.2657	229.1365	4	T	24	2598.1290	1299.5681
544.2977	272.6525	5	S	23	2497.0813	1249.0443
659.3246	330.1660	6	D	22	2410.0493	1205.5283
826.3230	413.6651	7	S	21	2295.0223	1148.0148
923.3757	462.1915	8	P	20	2128.0240	1064.5156
1020.4285	510.7179	9	P	19	2030.9712	1015.9893
1157.4874	579.2473	10	H	18	1933.9185	967.4629
1271.5303	636.2688	11	N	17	1796.8596	898.9334
1386.5573	693.7823	12	D	16	1682.8166	841.9120
1499.6413	750.3243	13	I	15	1567.7897	784.3985
1630.6818	815.8446	14	M	14	1454.7056	727.8565
1717.7139	859.3606	15	S	13	1323.6652	662.3362
1814.7666	907.8870	16	P	12	1236.6331	618.8202
1913.8350	957.4212	17	V	11	1139.5804	570.2938
2028.8620	1014.9346	18	D	10	1040.5119	520.7596
2125.9147	1063.4610	19	P	9	925.4850	463.2461
2182.9362	1091.9717	20	G	8	828.4322	414.7198
2282.0046	1141.5060	21	V	7	771.4108	386.2090
2353.0417	1177.0245	22	A	6	672.3424	336.6748
2481.1003	1241.0538	23	Q	5	601.3052	301.1563
2578.1531	1289.5802	24	P	4	473.2467	237.1270
2692.1960	1346.6016	25	N	3	376.1939	188.6006
2779.2280	1390.1177	26	S	2	262.1510	131.5791
		27	R	1	175.1190	88.0631

Figure S4. Related to Figure 6. FoxO1 Phosphorylation (continued)
(D) MS/MS spectra and b, y ion table of phosphorylated peptide #4 from *Camk2g*$^{-/-}$ HCs.

E

ELLTSDSPPHNDIMS$^{\Delta}$PVDPGVAQPNSR

$[M+2H]^{2+}$ m/z: 1478.15

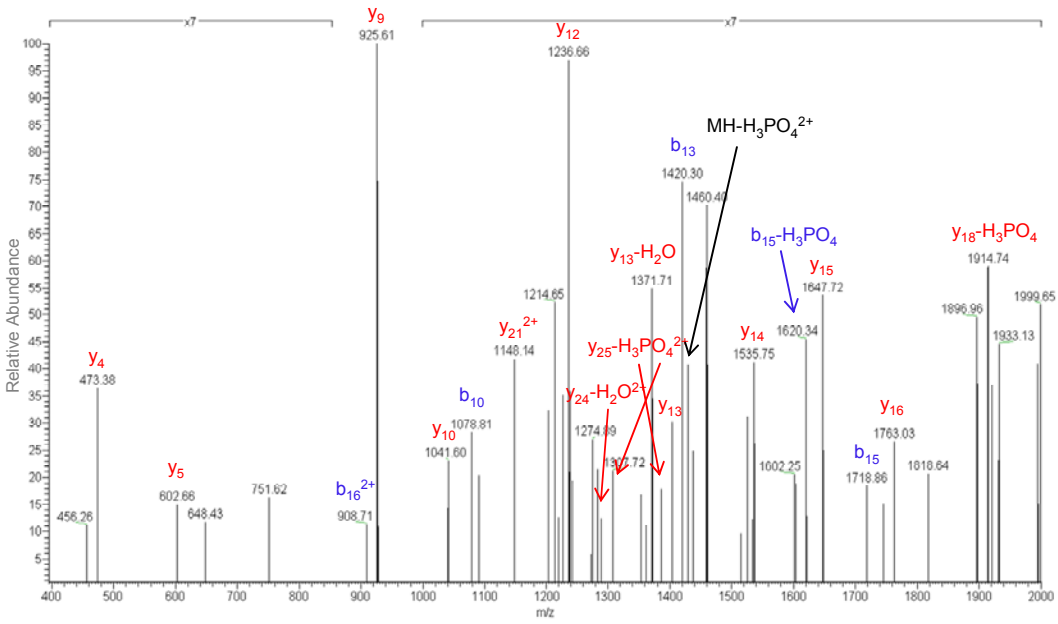

b+	b2+	#	Seq	#	y+	y2+
130.0499	65.5286	1	E	27		
243.1339	122.0706	2	L	26	2824.2971	1412.6522
356.2180	178.6126	3	L	25	2711.2131	1356.1102
457.2657	229.1365	4	T	24	2598.1290	1299.5681
544.2977	272.6525	5	S	23	2497.0813	1249.0443
659.3246	330.1660	6	D	22	2410.0493	1205.5283
746.3567	373.6820	7	S	21	2295.0223	1148.0148
843.4094	422.2084	8	P	20	2207.9903	1104.4988
940.4622	470.7347	9	P	19	2110.9375	1055.9724
1077.5211	539.2642	10	H	18	2013.8848	1007.4460
1191.5640	596.2857	11	N	17	1876.8259	938.9166
1306.5910	653.7991	12	D	16	1762.7829	881.8951
1419.6750	710.3412	13	I	15	1647.7560	824.3816
1550.7155	775.8614	14	M	14	1534.6719	767.8396
1717.7139	859.3606	15	S	13	1403.6315	702.3194
1814.7666	907.8870	16	P	12	1236.6331	618.8202
1913.8350	957.4212	17	V	11	1139.5804	570.2938
2028.8620	1014.9346	18	D	10	1040.5119	520.7596
2125.9147	1063.4610	19	P	9	925.4850	463.2461
2182.9362	1091.9717	20	G	8	828.4322	414.7198
2282.0046	1141.5060	21	V	7	771.4108	386.2090
2353.0417	1177.0245	22	A	6	672.3424	336.6748
2481.1003	1241.0538	23	Q	5	601.3052	301.1563
2578.1531	1289.5802	24	P	4	473.2467	237.1270
2692.1960	1346.6016	25	N	3	376.1939	188.6006
2779.2280	1390.1177	26	S	2	262.1510	131.5791
		27	R	1	175.1190	88.0631

F

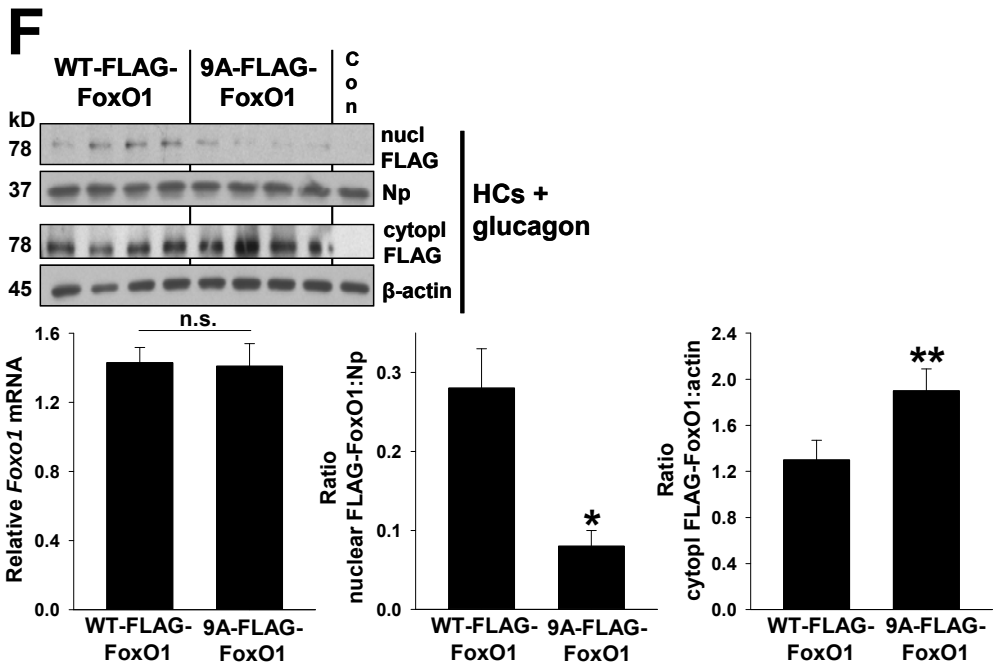

Figure S4. Related to Figure 6. FoxO1 Phosphorylation (continued)

(E) MS/MS spectra and b, y ion table of phosphorylated peptide #5 from *Camk2g*$^{-/-}$ HCs.

(F) Similar to the experiment in Fig. 6B, except the L-Foxo1 HCs were transfected with FLAG-9A-FoxO1 mutant instead of FLAG-7A-Foxo1 (*P = 0.006; **P = 0.02; mean ±S.E.M.).

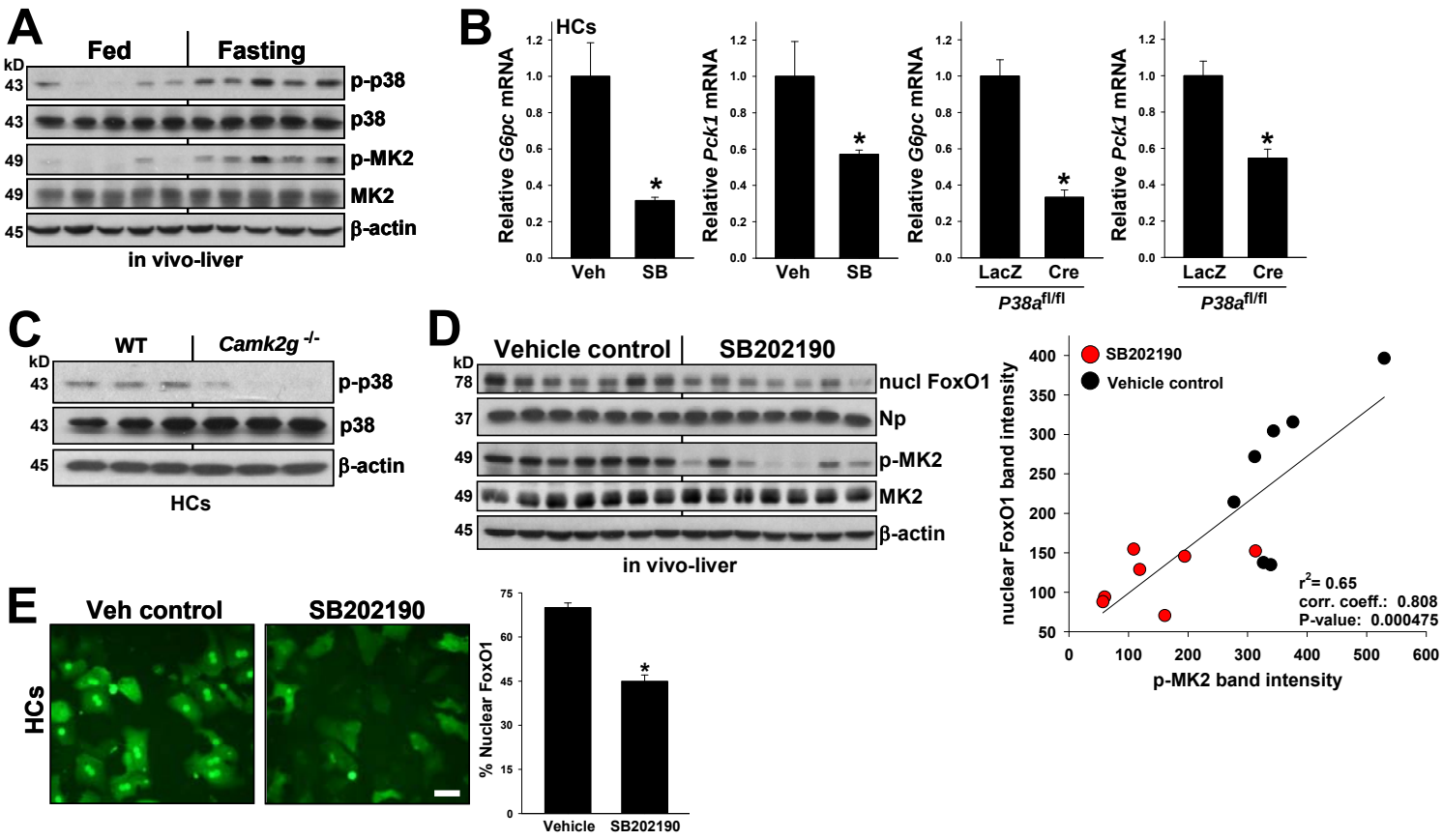

Figure S5. Related to Figure 6. p38

(A) Mice were fed ad libitum or fasted for 12 h. Liver phospho-p38, total p38, p-MK2, total MK-2, and β-actin were assayed by immunoblot.

(B) WT HCs were serum-depleted overnight and then incubated for 5 h with 100 nm glucagon in serum-free media with or without SB202190; or glucagon was added to HCs from *P38a*$^{fl/fl}$ mice treated with adeno-LacZ (control) or adeno-Cre. RNA was assayed for *G6pc* and *Pck1* mRNA (*P < 0.05; mean ± S.E.M.).

(C) HCs from fasting WT and *Camk2g*$^{-/-}$ mice were assayed for p-p38, total p38, and β-actin.

(D) WT mice were injected i.p. with 12.5 mg kg^{-1} body weight of p38 inhibitor (SB202190) or vehicle control. 12 h later, the mice were injected with an additional dose of SB202190 and fasted overnight. The livers were assayed for nuclear FoxO1, nucleophosmin, p-MK2, total MK-2, and β-actin. The correlation between nuclear FoxO1 and p-MK2 band intensities is shown in the graph.

(E) Adeno-GFP-FoxO1-transduced HCs were serum-depleted overnight, and then incubated for 5 h in serum-free media with SB202190 or vehicle (Veh) control. FoxO1 localization was assessed by indirect immunofluorescence (Bar, 10 μm; *P < 0.05; mean ± S.E.M.).

Supplemental Experimental Procedures

Reagents and Antibodies

Glucagon, pyruvate, forskolin, H89, 8-bromo-cAMP and SB202190 were from Sigma. BAPTA-AM and anti-nucleophosmin (Np) antibody were from Invitrogen. Xestospongin C was from EMD Chemicals. Anti–phospho-Thr287 CaMKII antibody was from Imgenex and Novus; anti–total CaMKII, anti-FoxO1 and anti-Ac-FoxO1 antibodies were from Santa Cruz Biotechnology Inc. Anti-β-actin and anti-phospho-S316 FoxO1 antibodies were from Abcam. Anti-phosho-p38, anti-phospho-MK2, anti-phospho-CREB, anti-p38, anti-MK2, anti-CREB, anti-phospho-T24 FoxO1, anti-phospho-S253 FoxO1, anti-HA and anti-FLAG antibodies were from Cell Signaling. Anti-CRTC2 antibody was a gift from Dr. Marc Montminy. Adenoviruses encoding LacZ, CA-CaMKII, KD-CaMKII, GFP-FoxO1, and Cre were described previously (Pfleiderer et al., 2004; Tanaka et al., 2009; Akagi et al., 1997) and amplified by Viraquest, Inc. (North Liberty, IA). Plasmids encoding FoxO1 mutants 7A and 9A were constructed as described (Asada et al., 2007).

Primary Hepatocytes

Primary mouse HCs were isolated from 8- to 12-week-old mice as described previously (Matsumoto et al., 2002). For most experiments, the HCs were serum-depleted overnight by incubation in medium containing 0.5% fetal calf serum and were then incubated for 5 h in serum-free media, with individual treatments noted in the figure legends. HCs were transduced with adenoviral constructs 12 h after plating, and experiments were conducted 24 h after transduction. Transfections with WT, 7A- and 9A-*Foxo1* were carried out using jetPEI™-hepatocyte DNA transfection reagent (Polyplus-transfection, Inc.) according to manufacturer's instructions.

Immunoprecipitation

Cells were lysed by a 5-min exposure to 1% Triton-X in 50 mM HEPES, 150 mM NaCl, 10 mM Na pyrophosphate, 10 mM EDTA, 10 mM EGTA, 1 mM Na3VO4, 50 mM NaF, 1 mM PMSF, and 5 μg/ml leupeptin. The lysate (500 μg of protein) was brought to a

total volume of 1 ml with lysis buffer containing 0.3–0.6 µg antibody and 80 µl Sepharose beads. The mixture was rotated in a 1.5-ml microfuge tube at 4°C for 14 h. Immune complexes were collected by centrifugation at 16,000 g and washed 3 times with chilled lysis buffer.

Generation of *Ip3r1*^{flox} Mice

The *Ip3r1*^{flox} mouse line was created in the Marks laboratory as follows: a targeting construct was generated by recombineering using the BAC clone RP24-245H16 (CHORI), containing a fragment of chromosome 6, encompassing exons 1 through 9 of IP_3R1 from C57Bl/6J mice (Liu et al., 2003; Warming et al., 2005). Plasmids pL451, pL452 & pL253 were kindly provided by Dr. Neal Copeland (NCI, NIH). Briefly, a Frt-Neo-Frt-loxP cassette (from plasmid pL451) was inserted upstream of exon 4 (second coding exon), then the Neo cassette was removed by agarose-induced flp recombination. The second and third loxP sites were introduced downstream of exon 4 by inserting loxP-Neo-loxP cassette (from vector pL452). Finally, a DTA cassette (from plasmid pL253), containing thymidine kinase, was inserted further downstream of the third loxP site. All intermediate BAC constructs and the final construct were screened by PCR, and the final construct was "fingerprinted" by Acc65I digestion and tested for loxP functionality. Crucial junction sites were confirmed by sequencing. The resulting modified BAC was electroporated into chimeric ES cells (CSL3 cell line, derived from 129S6/SvEvTac mouse line). The correct recombinant ES cells were injected into C57BL/6 blastocysts-stage mouse embryos. Chimeric male mice were bred to C57BL/6 female mice to establish a hybrid line. Germ-line transmission generated *Ip3r1*^{3xflox} mice, and females were crossed with EIIa-cre males to create *Ip3r1*^{flox} mice in which the floxed Neo cassette was eliminated. These mice were subsequently crossed with C57BL/6J mice to breed out the EIIa-cre allele. The final *Ip3r1*$^{fl/fl}$ line was derived through heterozygous breeding. Animal studies were performed in accordance with the Columbia University Animal Research Committee.

Immunoblotting and RT-qPCR

Immunoblot and RT-qPCR assays were performed as previously described (Timmins et al., 2009). Total RNA was extracted from HCs using the RNeasy kit (Qiagen). cDNA was synthesized from 2 µg total RNA using oligo (dT) and Superscript II (Invitrogen). Nuclear extraction from liver was performed using the Nuclear Extraction Kit from Panomics according to the manufacturer's instructions. With regard to anti-Thr287-p and total CaMKII immunoblots, we routinely saw 2 bands and occasionally 3 bands, which were absent in CaMKIIγ-deficient HCs. Whether their origin is alternative splicing or post-translational modification remains to be determined.

Mass Spectrometry of FoxO1 Phosphopeptides

HCs from WT and *Camk2g*$^{-/-}$ mice were transduced with adeno-FLAG-FoxO1 at an MOI of 2. Cells were serum-depleted overnight and then incubated for 5 h in serum-free media. FoxO1 was immunopurified using anti-FLAG. FLAG-FoxO1 in ice-cold Tris-buffered saline was precipitated by mixing 1 volume of the sample solution (cold) with 1/3 volume of 100% (w/v) TCA (6.1 N, Sigma). After 3 h on ice, the samples were centrifuged for 30 min at 4°C, and the supernate was aspirated leaving ~5-10 µl in the tube so as to not disturb the pellet. The pellet was washed twice with ice-cold acetone (500 µl each). After each wash, the solution was centrifuged for 10 min. The final pellet was then dried on a Speed-vac for 1-2 min.

Peptides were generated by proteolysis as described (Delahunty and Yates, III, 2005; MacCoss et al., 2002). The TCA pellets were solubilized in 60 µl of 100 mM Tris-HCl, pH 8.5, containing 8 M urea, and then the proteins were reduced by the addition of 500 mM Tris (2-carboxyethyl)phosphine (TCEP) to a final concentration of 5 mM. After a 20-min incubation at room temperature, cysteine residues were carboxymethylated by the addition of 500 mM iodoacetamide to achieve a final concentration of 10 mM. The solution was incubated for 30 min at room temperature in the dark and then split equally into three tubes. In one of the tubes, the concentration of urea was then diluted 2-fold (to 4 M) by the addition of an equal volume of 100 mM Tris-HCl, pH 8.5, and then subtilisin (Promega) was added at ~1:100 enzyme:substrate ratio (wt:wt) and incubated at 37°C for 4 h in the dark. The other two samples were diluted 4-fold (to 2 M), and

elastase and trypsin (Promega) were added at ~1:100 enzyme:substrate ratio (wt:wt), and then both samples were incubated at 37°C overnight in the dark. The resulting peptides from the three digests were combined into one tube and dissolved in 90% formic acid to a final concentration of 2% in 10% acetonitrile. The samples were stored at -20°C prior to TiO2 enrichment and LC-MS/MS analysis.

TiO2 enrichment for phosphopeptides was done as described by Cantin *et al.* (Cantin et al., 2007). A TiO2 column was made by pressure-slurry packing TiO2 (5-μ partisphere, Whatman, Clifton, NJ) into fused-silica capillary (250-μm i.d.) to a length of 5 cm, and the peptide mixtures were pressure-loaded onto the column. The column was washed with buffer A and B (see the following section for buffer compositions) in succession, and then phosphopeptides were eluted using 250 mM ammonium bicarbonate (pH 9) directly into 100-μm-i.d. Kasil-fritted end packed column with 5 cm of 5-μm reversed phase (Gemini C18, Phenomenex, Torrance, CA), which was linked to a pulled-tip analytical column with a bed volume of 15 cm of the same reversed phase. This second column was in-line with an Agilent 1200 quaternary HPLC pump (Palo Alto, CA) for mass spectrometry analysis.

The HPLC buffer solutions used were water/acetonitrile/formic acid (95:5:0.1, v/v/v) as buffer A and water/acetonitrile/ formic acid (20:80:0.1, v/v/v) as buffer B. The elution gradient was as follows: 10 min of 100% buffer A, a 5-min gradient from 0 to 15% buffer B, a 65-min gradient from 15 to 45% buffer B, a 15-min gradient from 45 to 100% buffer B, and 5 min of 100% buffer B. Data-dependent tandem mass spectrometry (MS/MS) analysis was performed with a LTQ-Velos-Orbitrap mass spectrometer (ThermoFisher, San Jose, CA). Peptides eluted from the LC column were directly electrosprayed into the mass spectrometer with the application of a distal 2.5-kV spray voltage. A cycle of one full-scan MS spectrum (m/z 300-1800) was acquired followed by twenty MS/MS events, sequentially generated on the first to the twentieth most intense ions selected from the full MS spectrum at a 35% normalized collision energy. The number of microscans was one for both MS and MS/MS scans, and the maximum ion injection time was 25 and 50 ms respectively. The dynamic exclusion settings used were as follows: repeat count, 1; repeat duration, 30 second; exclusion

list size, 500; and exclusion duration, 120 second. MS scan functions and HPLC solvent gradients were controlled by the Xcalibur data system (ThermoFisher).

G6PC Promoter-Luciferase Assay

FAO hepatocytes were transfected with a construct encoding nucleotides -1227 to +57 of the human *G6PC* promoter fused to luciferase (-1227 WT) or the same construct with three consensus FoxO binding sites mutated (-1227 Mut): -187 to -183 (GTTT $\rightarrow$ CGAG); -171 (G $\rightarrow$ C); and -164 (A $\rightarrow$ C), disrupting the consensus IRS sequences T(G/A)TTT in the *G6PC* promoter (Ayala et al., 1999; von Groote-Bidlingmaier et al., 2003). The final mutation at position -164 is upstream of the cAMP-response element (CRE; -161 to -152), leaving the CRE unaffected (Barthel et al., 2001). Hepatocytes were treated for 16 h with 0.1 mM cAMP and 1 μM dexamethasone in serum-free medium with 1% BSA prior to lysis and analysis of luciferase activity. The luciferase units (RLU) were normalized to the untreated cells in each group.

SUPPLEMENTAL REFERENCES

Akagi,K., Sandig,V., Vooijs,M., van,d., V, Giovannini,M., Strauss,M., and Berns,A. (1997). Cre-mediated somatic site-specific recombination in mice. Nucleic Acids Res. *25*, 1766-1773.

Asada,S., Daitoku,H., Matsuzaki,H., Saito,T., Sudo,T., Mukai,H., Iwashita,S., Kako,K., Kishi,T., Kasuya,Y., and Fukamizu,A. (2007). Mitogen-activated protein kinases, Erk and p38, phosphorylate and regulate Foxo1. Cell Signal. *19*, 519-527.

Ayala,J.E., Streeper,R.S., Desgrosellier,J.S., Durham,S.K., Suwanichkul,A., Svitek,C.A., Goldman,J.K., Barr,F.G., Powell,D.R., and O'Brien,R.M. (1999). Conservation of an insulin response unit between mouse and human glucose-6-phosphatase catalytic subunit gene promoters: transcription factor FKHR binds the insulin response sequence. Diabetes. *48*, 1885-1889.

Barthel,A., Schmoll,D., Kruger,K.D., Bahrenberg,G., Walther,R., Roth,R.A., and Joost,H.G. (2001). Differential regulation of endogenous glucose-6-phosphatase and phosphoenolpyruvate carboxykinase gene expression by the forkhead transcription factor FKHR in H4IIE-hepatoma cells. Biochem. Biophys. Res. Commun. *285*, 897-902.

Cantin,G.T., Shock,T.R., Park,S.K., Madhani,H.D., and Yates,J.R., III (2007). Optimizing TiO2-based phosphopeptide enrichment for automated multidimensional liquid chromatography coupled to tandem mass spectrometry. Anal. Chem. *79*, 4666-4673.

Delahunty,C. and Yates,J.R., III (2005). Protein identification using 2D-LC-MS/MS. Methods. *35*, 248-255.

Liu,P., Jenkins,N.A., and Copeland,N.G. (2003). A highly efficient recombineering-based method for generating conditional knockout mutations. Genome Res. *13*, 476-484.

MacCoss,M.J., McDonald,W.H., Saraf,A., Sadygov,R., Clark,J.M., Tasto,J.J., Gould,K.L., Wolters,D., Washburn,M., Weiss,A., Clark,J.I., and Yates,J.R., III (2002). Shotgun identification of protein modifications from protein complexes and lens tissue. Proc Natl Acad Sci U S A. *99*, 7900-7905.

Matsumoto,M., Ogawa,W., Teshigawara,K., Inoue,H., Miyake,K., Sakaue,H., and Kasuga,M. (2002). Role of the insulin receptor substrate 1 and phosphatidylinositol 3-kinase signaling pathway in insulin-induced expression of sterol regulatory element binding protein 1c and glucokinase genes in rat hepatocytes. Diabetes. *51*, 1672-1680.

Pfleiderer,P.J., Lu,K.K., Crow,M.T., Keller,R.S., and Singer,H.A. (2004). Modulation of vascular smooth muscle cell migration by calcium/ calmodulin-dependent protein kinase II-delta 2. Am J Physiol Cell Physiol *286*, C1238-C1245.

Tanaka,J., Li,Q., Banks,A.S., Welch,C.L., Matsumoto,M., Kitamura,T., Ido-Kitamura,Y., Depinho,R.A., and Accili,D. (2009). Foxo1 links hyperglycemia to LDL oxidation and eNOS dysfunction in vascular endothelial cells. Diabetes.

Timmins,J.M., Ozcan,L., Seimon,T.A., Li,G., Malagelada,C., Backs,J., Backs,T., Bassel-Duby,R., Olson,E.N., Anderson,M.E., and Tabas,I. (2009). Calcium/calmodulin-dependent protein kinase II links endoplasmic reticulum stress with Fas and mitochondrial apoptosis pathways. J. Clin. Invest. *119*, 2925-2941.

von Groote-Bidlingmaier,F., Schmoll,D., Orth,H.M., Joost,H.G., Becker,W., and Barthel,A. (2003). DYRK1 is a co-activator of FKHR (FOXO1a)-dependent glucose-6-phosphatase gene expression. Biochem. Biophys. Res. Commun. *300*, 764-769.

Warming,S., Costantino,N., Court DL, Jenkins,N.A., and Copeland,N.G. (2005). Simple and highly efficient BAC recombineering using galK selection. Nucleic Acids Res. *33*, e36.